Microbial byproducts determine reproductive fitness of free-living and parasitic nematodes

Mericien Venzon[*1,2], Ritika Das[*2,4], Daniel J. Luciano[2,5], Hyun Shin Park[6], Eric T. Kool[7], Joel G. Belasco[2,5], E. Jane Albert Hubbard[2,3,4,†], Ken Cadwell[2,5,8,†]

1. Vilcek Institute of Graduate Biomedical Sciences, New York University Grossman School of Medicine, New York, NY, USA
2. Kimmel Center for Biology and Medicine at the Skirball Institute, New York University Grossman School of Medicine, New York, NY, USA
3. Department of Pathology, New York University Grossman School of Medicine, New York, NY, USA
4. Department of Cell Biology, New York University Grossman School of Medicine, New York, NY, USA
5. Department of Microbiology, New York University Grossman School of Medicine, New York, NY, USA
6. Seegene Inc., Ogeum-ro, Songpa-Gu, Seoul, Republic of Korea
7. Department of Chemistry, Stanford Cancer Institute and ChEM-H Institute, Stanford University, Stanford, CA, USA
8. Division of Gastroenterology, Department of Medicine, New York University Grossman School of Medicine, New York, NY, USA

* These authors contributed equally

[†]Co-corresponding, equal contribution

Correspondence:

jane.hubbard@nyulangone.org

ken.cadwell@nyulangone.org

Abstract

Trichuris nematodes reproduce within the microbiota-rich mammalian intestine, yet microbial byproducts that facilitate the parasite lifecycle are unknown. Here, we report a novel pipeline to identify microbial factors with conserved roles in the reproduction of nematodes. A screen for *E. coli* mutants that impair *C. elegans* fertility identified genes in fatty acid biosynthesis and ethanolamine utilization pathways, including *fabH* and *eutN*. *Trichuris muris* eggs displayed defective hatching in the presence of *E. coli* deficient in *fabH* or *eutN* due to reduction in arginine or elevated levels of aldehydes, respectively. Remarkably, *T. muris* reared in gnotobiotic mice colonized with these *E. coli* mutants failed to lay viable eggs. These findings indicate that microbial byproducts mediate evolutionarily conserved transkingdom interactions that impact reproductive fitness of distantly-related nematodes.

One-Sentence Summary: Byproducts from the microbiota contribute to the life cycles of distantly-related free-living and parasitic worms.

Main text

The reproductive success of the parasitic nematode *Trichuris trichuira* is evidenced by the over 400 million individuals colonized by this soil-transmitted helminth (*1*). Its enormous reproductive capacity contributes to its infectious spread and hampers parasite eradication efforts. A distinct feature of *Trichuris* species is that reproductive development, from egg hatching to egg laying, is completed exclusively within the host digestive tract (*2, 3*). A new infection begins when embryonated eggs ingested from the environment hatch in the host cecum, a region within the gastrointestinal tract populated by a dense community of bacteria. Although bacteria mediate egg hatching for *Trichuris muris* (*4-6*), the *Trichuris* species that infects mice, a role for bacteria at later stages of *Trichuris* development remains unclear. Our group and others have shown that *Trichuris* infections in mice and humans affect the bacterial composition of the gut microbiota (*6-13*). Additionally, the *T. muris* microbiota harbors taxa similar to those observed in the murine host microbiota, with a notable enrichment of Proteobacteria, including Gram-negative commensals like *E. coli* (*6*).

For the free-living nematode *C. elegans*, reducing the quantity or quality of the bacterial diet, or interfering with nutrient uptake, can impair germline development with consequences for fertility (*14-19*). Because of the high degree of conservation of body plan and neuromuscular system organization within the phylum Nematoda, *C. elegans* has been used as a model for the discovery of anthelmintics for more than four decades (*20, 21*). Therefore, we hypothesized that bacteria-derived essential requirements for reproductive development in the well-characterized, model organism *C. elegans* are conserved in *Trichuris*.

To identify bacteria-derived factors that impact nematode reproduction, we assessed fertility of young adult *C. elegans* raised on a library of viable *E. coli* mutants. We used *C. elegans* bearing a temperature-sensitive mutation in the gene encoding the GLP-1 Notch receptor, *glp-1(e2141),* to facilitate quantification of fertility. At the semi-permissive temperature of 20ºC, the number of germline progenitor cells is roughly half of the wild type (*22*), thereby sensitizing the worms to fertility defects when signaling pathways conveying nutritional sufficiency are altered (*14, 18*). The *C. elegans* strain also carried fluorescent markers for the pharynx and for embryos (*23*) to facilitate counting and staging the worms, and to determine whether individual worms contained embryos (gravid) (Fig. 1, A-B). Wells were excluded from subsequent analyses if *E. coli* failed to grow, or if *C. elegans* exhibited developmental arrest or severely delayed growth. Using a series of selection criteria that considered both plate-by-plate statistical comparisons and penetrance, our primary screen of ~3000 of the 3985 *E. coli* mutants in the Keio library identified 315 bacterial mutants that reduced the percentage of gravid worms at the established time point (Fig. 1, C-D).

After these 315 *E. coli* mutants were re-screened in biological triplicate, ten mutants significantly reduced the penetrance of embryo-bearing *C. elegans* compared to our wild-type (WT) *E. coli* strain (GC1547) in at least two out of three biological replicates (Fig. 1C and S1, A-B). Seven of the ten *E. coli* genes fell into three functional groups related to ethanolamine utilization, fatty acid biosynthesis or lipopolysaccharide synthesis (Table S1).

We focused on the *E. coli* mutants *ΔfabF, ΔfabH, ΔeutD,* and *ΔeutN*, because they were associated with the greatest reduction in embryo-bearing *C. elegans* (Fig.

1E). Complementation with a plasmid carrying the wild-type *fabH* or *eutN* sequences confirmed their functional relevance in the *C. elegans* fertility delay phenotype (Fig. S1C). For *fabF*, we rederived the *E. coli* deletion mutant by using P1 phage to transduce the original Δ*fabF*::*kan* allele from the Keio library strain into the Keio progenitor strain BW25113 (Fig. S1, D-E). Similar to the original mutant, the transductant caused a significant reduction in the percentage of embryo-bearing *C. elegans*.

To assess whether these *E. coli* mutants delayed somatic and/or germline development of *C. elegans*, we performed a time-course analysis of vulval development (*24*) and assayed for enhancement of the Pro phenotype caused by a weak *glp-1(gf)* mutation (*25*). The latter assay is a proxy for delayed germline development relative to somatic development (*26*). Among the four mutants, only worms fed *ΔeutN* exhibited delayed somatic development, with an additional germline delay relative to somatic development (Fig. 1, F-G). Worms fed *ΔfabF* displayed delayed germline development without the somatic delay, while *ΔfabH* and *ΔeutD* developed comparably with worms fed WT *E. coli*. When we prolonged the assay by scoring the worms on Day 2—24 hours after the initial screening time-point (Day 1)—the percentage of gravid worms significantly increased, indicating that feeding on these *E. coli* mutants delayed *C. elegans* fertility rather than induced permanent sterility (Fig. 1H). We also found no significant differences when comparing the number of germline progenitor zone (PZ) nuclei in *C. elegans* raised on each mutant or WT *E. coli* at the L4-to-adult molt (Fig. S1, F-G), indicating that the delay in fertility is not likely due to slower accumulation of the PZ during larval stages (*14, 27, 28*).

DAF-2 insulin/IGF-like and DAF-7 TGFß signaling pathways link nutrition and fertility (*16-18, 22*). However, constitutive activation of these pathways (by loss of DAF-16 FOXO or DAF-5, respectively) did not substantially mitigate the delay in fertility caused by the *E. coli* mutants. Loss of *daf-16* actually exacerbated the penetrance of non-gravid worms, even with WT *E. coli* (Fig. S1H), whereas constitutive activation of the DAF-7 TGFß pathway via loss of *daf-5* had no effect on fertility of *C. elegans* raised on *ΔeutD* and a modest effect with *ΔeutN*, *ΔfabF* and *ΔfabH* (Fig. S1I). Loss of *daf-5* also elevated penetrance of gravid *C. elegans* raised on WT *E. coli* to a similar or greater extent. We conclude that neither pathway likely mediates the effects of these *E. coli* mutants on the timing of *C. elegans* fertility.

Having identified *E. coli* mutants that impede fertility of a free-living nematode, we examined whether these bacteria impact a distantly-related parasitic nematode. *T. muris* egg hatching was shown to be the reproductive stage sensitive to the presence of bacteria (*4, 6*). Thus, to begin investigating possible effects of the mutants identified in our *C. elegans* screen on the *Trichuris* lifecycle, we adapted a previously described method to quantify *E. coli*-mediated hatching kinetics of embryonated *T. muris* eggs *in vitro* (*4*) (Fig. 2A). All *E. coli* mutants were confirmed to have similar growth kinetics to WT *E. coli* (Fig. S2). Two of the mutants tested, *ΔeutN* and *ΔfabH,* elicited significantly reduced hatching compared to rates mediated by WT *E. coli* (Fig. 2B). Complementation of *ΔeutN* or *ΔfabH* with their wild-type genes rescued hatching (Fig. S3).

To determine whether reduced egg hatching is due to the production of a toxic factor, we performed the hatching assay utilizing WT *E. coli* mixed with each mutant in a

9:1 or 1:1 ratio (Fig. 2C). As little as 10% *ΔeutN* in the mixture significantly inhibited the ability of WT *E. coli* to mediate hatching, whereas the presence of *ΔfabH* had no effect. Thus, the inhibitory effect of *ΔeutN* is dominant over WT *E. coli*, implicating the production of a toxic factor by this mutant, while the reduced hatching rate of embryonated eggs incubated with *ΔfabH* is likely due to deficiency of a pro-hatching factor.

Hybrid metabolomics revealed an unexpectedly low relative level of arginine and ornithine in *ΔfabH* cell lysates compared to WT *E. coli* (Fig. 2D). Supplementation of *ΔfabH* cultures with 500μM arginine partly suppressed the *C. elegans* fertility delay without elevating the baseline fertility seen in the control (Fig. 2E and S4, A-B). We observed a similar result with ornithine supplementation (Fig. 2F and S4C). Supplementation of *ΔfabH* cultures with arginine or ornithine also successfully rescued *T. muris* egg hatching to levels similar to WT *E. coli* (Fig. 2, G-H and S4, D-E). Consistent with a role for the arginine biosynthesis pathway, we found that *Trichuris* egg hatching was diminished in the presence of *ΔargE* or *ΔargH E. coli*, mutants defective in ornithine and arginine synthesis, respectively (Fig. 2, I-J).

Although optimal *T. muris* egg hatching *in vitro* requires physical contact with *E. coli (4, 5)*, a reduced amount of hatching can still occur in a transwell system that separates bacteria and eggs into different chambers (*5*), suggesting that both contact-dependent and independent factors contribute to the process. Similar to previous reports, eggs hatched at approximately 50% their maximum rate when incubated separately from WT *E. coli* in a transwell system (Fig. 2, K-L). Hatching was further reduced when *ΔfabH* was used as the bacterium. Supplementation of ornithine restored

158 hatching in the presence of *ΔfabH* to levels similar to those elicited by WT *E. coli* in the
159 transwell system. Altogether, these findings indicate that nematode pathways regulated
160 by ornithine and arginine contribute to contact-independent *E. coli*-mediated hatching of
161 *T. muris* embryonated eggs.

162 To understand why *T. muris* eggs incubated with *ΔeutN E. coli* displayed the
163 greatest reduction in hatching, we first determined whether disrupting other parts of the
164 ethanolamine utilization pathway (Fig. 3A) led to similar outcomes. *E. coli* mutants
165 lacking enzymes in the pathway—*ΔeutB*, *ΔeutC*, *ΔeutD*, *ΔeutE*, and *ΔeutG*—facilitated
166 egg hatching at rates similar to WT *E. coli* (Fig. 3B). In contrast to these *eut* operon
167 genes, *eutN* encodes a subunit of a proteinaceous shell that enables the efficient
168 colocalization of the *eut* enzymes with their cofactors and substrates within a
169 microcompartment and prevents diffusion of pathway intermediates (*29*). It is possible
170 that disruption of the microcompartment architecture allows the release of a soluble
171 toxic intermediate. Therefore, we tested whether transferring the supernatant from
172 *ΔeutN* culture was sufficient to inhibit the ability of WT *E. coli* to mediate hatching (Fig.
173 3C). Although transferring culture supernatant from *ΔeutN* grown in isolation had no
174 effect, supernatant isolated from *ΔeutN* that had been incubated with eggs reduced
175 hatching mediated by WT *E. coli* (Fig. 3D). This suggests that *ΔeutN* produces a soluble
176 toxic factor in the presence of *T. muris* embryonated eggs.

177 Acetaldehyde is a known intermediate of the ethanolamine utilization pathway
178 that can readily form irreversible adducts with proteins, changing their conformation and
179 function (*30, 31*). Additionally, deletion of *eutN* in *Salmonella* resulted in the greatest
180 increase in acetaldehyde volatility among all *eut* operon mutants during the first hours of

growth (*32*). Using a fluorogenic hydrazone transfer (DarkZone) system to label aldehydes (*33*), we detected elevated levels of aldehydes in the culture supernatant of *ΔeutN* that had been incubated with *T. muris* eggs, but not in the culture supernatant of the complemented *ΔeutN* strain or when the mutant was grown in the absence of eggs (Fig. 3E and S5A). Aldehyde levels were also elevated in *ΔeutD,* the other *E. coli* mutant of this pathway identified by the *C. elegans* screen, although the increase following egg incubation was not as striking as for *ΔeutN*, potentially explaining why deletion of *eutD* did not inhibit hatching (Fig. 3E). Next, we deleted the rate limiting enzyme of the ethanolamine utilization pathway, *eutC*, in the *ΔeutN* background (*ΔeutNΔeutC)* to prevent the formation of toxic intermediates (*32, 34*). We found that aldehyde levels of *ΔeutNΔeutC* were similar to that of WT *E. coli* and that *T. muris* egg hatching was completely restored when the assay was performed with this double mutant (Fig. 3E-F). Additionally, we found that supplementation with acetaldehyde was sufficient to inhibit hatching elicited by WT *E. coli* in a concentration-dependent manner and confirmed that bacteria viability was unaffected (Fig. S5, B-C).

In vitro T. muris egg hatching serves as a sensitive assay to investigate nematode-bacteria interactions, but the role of intestinal bacteria in subsequent steps of *Trichuris* development remains obscure because they are difficult to recreate outside the mammalian host. Given that the *C. elegans* screen was focused on development of the reproductive tract, we established a bacterial monocolonization mouse model to investigate the role of bacterial *fabH*, *eutN*, and *eutD* in *T. muris* development and reproduction (Fig. 4A). After we verified that each *E. coli* mutant colonized germ-free mice to levels similar to WT *E. coli* (Fig. S6A), monocolonized mice were gavaged twice

with 100 eggs and sacrificed two weeks after the second gavage. We were able to recover adult worms from the cecum of mice monocolonized with WT *E. coli* but not germ-free mice (Fig. S6B), consistent with previous observations (*6*), indicating that our assay allows investigation of mechanisms by which *E. coli* contributes to *T. muris* development in an intact host. Our experimental setup in which mice receive high doses of embryonated eggs was designed to overcome the potential reduced hatching efficiency that may occur in mice lacking a complex microbiota. Therefore, as expected, we did not detect any differences in worm burden when comparing mice colonized with WT *E. coli* versus *⊿fabH*, *⊿eutN*, and *⊿eutD* strains (Fig. S6B). However, many of the *T. muris* recovered from mice colonized with these mutants displayed a striking deformity characterized by shortened length (Fig. 4, B-C; indicated by arrowheads). Although worms from WT *E. coli*-colonized mice were exclusively long in length, mice colonized with *⊿fabH*, *⊿eutN*, and *⊿eutD E. coli* produced a mixture of both long and short length worms, defined as < 1cm. The defect was most severe in mice monocolonized with *⊿eutN* from which most worms recovered were short.

The average number of freshly laid eggs per worm was not significantly different between the conditions (Figure S6C). However, in stark contrast to worms from WT *E. coli*-colonized mice, which laid eggs of the typical ovoid structure, eggs laid by worms harvested from mice colonized with *⊿fabH*, *⊿eutD*, and *⊿eutN E. coli* displayed an aberrant rounded morphology, and in some cases lacked opercula and a distinct shell, and the inner contents were disorganized (Fig. 4, D-E). These structurally aberrant eggs took longer to reach embryonated morphology, and even after a prolonged incubation period, significantly fewer eggs appeared embryonated in the *⊿eutN* and *⊿eutD* groups

(Fig. 4F). Eggs laid by worms from all three mutant-colonized groups of mice had significantly lower hatching rates compared to eggs laid by worms from WT *E. coli*-colonized mice when tested for bacteria-mediated hatching *in vitro* (Fig. 4G). Finally, monocolonization with *ΔeutNΔeutC* abrogated the length and egg fitness defects of *T. muris* observed in *ΔeutN*-colonized mice (Fig. S7). Thus, bacterial products are important for the reproductive development of *T. muris in vivo*.

Despite the wide taxonomic divergence between *C. elegans* and *T. muris*, our screen for bacterial factors impacting fertility in *C. elegans* identified two pathways that impact *T. muris* biology. Our finding that bacterial deficiencies decrease *T. muris* worm size and egg fitness is in line with recent evidence showing that another parasitic nematode *Heligmosomoides polygyrus*, lays fewer eggs and exhibits similar length defects when reared in a germ-free host (*35*). Our results also provide evidence for a previously undescribed role for byproducts of microbial metabolism on nematode development, a role that appears evolutionarily conserved. Despite lacking many genes specific to parasitism, our findings support the utility of *C. elegans* as a model for bacteria-nematode interactions because of its high sensitivity to its bacterial milieu. Focusing on microbiota-nematode interactions has also revealed vulnerabilities of *Trichuris* that have implications for transmission dynamics and may be useful for controlling life-long infections in areas where helminths are endemic because of ineffective deworming treatment and high rates of reinfection. We propose that *C. elegans* can be used as a novel system for investigating the effects of specific microbial genes and pathways in supporting the parasitic nematode life cycle and aid in further understanding the transkingdom interactions that sustain human disease.

References

1. G. B. D. Disease, I. Injury, C. Prevalence, Global, regional, and national incidence, prevalence, and years lived with disability for 310 diseases and injuries, 1990-2015: a systematic analysis for the Global Burden of Disease Study 2015. *Lancet* **388**, 1545-1602 (2016).
2. M. A. Fahmy, An investigation on the life cycle of Trichuris muris. *Parasitology* **44**, 50-57 (1954).
3. T. Panesar, The moulting pattern in Trichuris muris (Nematoda: Trichuroidea). *Canadian journal of zoology* **67**, 2340-2343 (1989).
4. K. S. Hayes *et al.*, Exploitation of the intestinal microflora by the parasitic nematode Trichuris muris. *Science* **328**, 1391-1394 (2010).
5. K. Koyama, Bacteria-induced hatching of Trichuris muris eggs occurs without direct contact between eggs and bacteria. *Parasitol Res* **115**, 437-440 (2016).
6. E. C. White *et al.*, Manipulation of host and parasite microbiotas: Survival strategies during chronic nematode infection. *Sci Adv* **4**, eaap7399 (2018).
7. D. Ramanan *et al.*, Helminth infection promotes colonization resistance via type 2 immunity. *Science* **352**, 608-612 (2016).
8. B. A. Rosa *et al.*, Whipworm-Associated Intestinal Microbiome Members Consistent Across Both Human and Mouse Hosts. *Front Cell Infect Microbiol* **11**, 637570 (2021).
9. S. C. Lee *et al.*, Helminth colonization is associated with increased diversity of the gut microbiota. *PLoS Negl Trop Dis* **8**, e2880 (2014).
10. T. P. Jenkins *et al.*, Infections by human gastrointestinal helminths are associated with changes in faecal microbiota diversity and composition. *PLoS One* **12**, e0184719 (2017).
11. J. B. Holm *et al.*, Chronic Trichuris muris Infection Decreases Diversity of the Intestinal Microbiota and Concomitantly Increases the Abundance of Lactobacilli. *PLoS One* **10**, e0125495 (2015).

12. A. Houlden *et al.*, Chronic Trichuris muris Infection in C57BL/6 Mice Causes Significant Changes in Host Microbiota and Metabolome: Effects Reversed by Pathogen Clearance. *PLoS One* **10**, e0125945 (2015).
13. J. Schachter *et al.*, Whipworm Infection Promotes Bacterial Invasion, Intestinal Microbiota Imbalance, and Cellular Immunomodulation. *Infect Immun* **88**, (2020).
14. D. Z. Korta, S. Tuck, E. J. Hubbard, S6K links cell fate, cell cycle and nutrient response in C. elegans germline stem/progenitor cells. *Development* **139**, 859-870 (2012).
15. X. Gracida, C. R. Eckmann, Fertility and germline stem cell maintenance under different diets requires nhr-114/HNF4 in C. elegans. *Curr Biol* **23**, 607-613 (2013).
16. T. A. Starich, X. Bai, D. Greenstein, Gap junctions deliver malonyl-CoA from soma to germline to support embryogenesis in Caenorhabditis elegans. *Elife* **9**, (2020).
17. O. Pekar *et al.*, Linking the environment, DAF-7/TGFbeta signaling and LAG-2/DSL ligand expression in the germline stem cell niche. *Development* **144**, 2896-2906 (2017).
18. D. Dalfo, D. Michaelson, E. J. Hubbard, Sensory regulation of the C. elegans germline through TGF-beta-dependent signaling in the niche. *Curr Biol* **22**, 712-719 (2012).
19. B. Spanier *et al.*, The Reproduction Rate of Peptide Transporter PEPT-1 Deficient C. elegans Is Dependent on Dietary Glutamate Supply. *Front Mol Biosci* **5**, 109 (2018).
20. D. Sepulveda-Crespo, R. M. Reguera, F. Rojo-Vazquez, R. Balana-Fouce, M. Martinez-Valladares, Drug discovery technologies: Caenorhabditis elegans as a model for anthelmintic therapeutics. *Med Res Rev* **40**, 1715-1753 (2020).
21. G. Salinas, G. Risi, Caenorhabditis elegans: nature and nurture gift to nematode parasitologists. *Parasitology* **145**, 979-987 (2018).
22. D. Michaelson, D. Z. Korta, Y. Capua, E. J. Hubbard, Insulin signaling promotes germline proliferation in C. elegans. *Development* **137**, 671-680 (2010).

23. D. Roy, D. J. Kahler, C. Yun, E. J. A. Hubbard, Functional Interactions Between rsks-1/S6K, glp-1/Notch, and Regulators of Caenorhabditis elegans Fertility and Germline Stem Cell Maintenance. *G3 (Bethesda)* **8**, 3293-3309 (2018).
24. D. Z. Mok, P. W. Sternberg, T. Inoue, Morphologically defined sub-stages of C. elegans vulval development in the fourth larval stage. *BMC Dev Biol* **15**, 26 (2015).
25. A. S. Pepper, T. W. Lo, D. J. Killian, D. H. Hall, E. J. Hubbard, The establishment of Caenorhabditis elegans germline pattern is controlled by overlapping proximal and distal somatic gonad signals. *Dev Biol* **259**, 336-350 (2003).
26. E. J. A. Hubbard, T. Schedl, Biology of the Caenorhabditis elegans Germline Stem Cell System. *Genetics* **213**, 1145-1188 (2019).
27. I. Agarwal *et al.*, HOP-1 Presenilin Deficiency Causes a Late-Onset Notch Signaling Phenotype That Affects Adult Germline Function in Caenorhabditis elegans. *Genetics* **208**, 745-762 (2018).
28. Z. Kocsisova, K. Kornfeld, T. Schedl, Rapid population-wide declines in stem cell number and activity during reproductive aging in C. elegans. *Development* **146**, (2019).
29. T. O. Yeates, C. S. Crowley, S. Tanaka, Bacterial microcompartment organelles: protein shell structure and evolution. *Annu Rev Biophys* **39**, 185-205 (2010).
30. M. F. Sorrell, D. J. Tuma, The functional implications of acetaldehyde binding to cell constituents. *Ann N Y Acad Sci* **492**, 50-62 (1987).
31. T. M. Donohue, Jr., D. J. Tuma, M. F. Sorrell, Acetaldehyde adducts with proteins: binding of [14C]acetaldehyde to serum albumin. *Arch Biochem Biophys* **220**, 239-246 (1983).
32. J. T. Penrod, J. R. Roth, Conserving a volatile metabolite: a role for carboxysome-like organelles in Salmonella enterica. *J Bacteriol* **188**, 2865-2874 (2006).
33. L. H. Yuen, N. S. Saxena, H. S. Park, K. Weinberg, E. T. Kool, Dark Hydrazone Fluorescence Labeling Agents Enable Imaging of Cellular Aldehydic Load. *ACS Chem Biol* **11**, 2312-2319 (2016).

34. D. M. Roof, J. R. Roth, Functions required for vitamin B12-dependent ethanolamine utilization in Salmonella typhimurium. *J Bacteriol* **171**, 3316-3323 (1989).
35. S. Rausch *et al.*, Parasitic Nematodes Exert Antimicrobial Activity and Benefit From Microbiota-Driven Support for Host Immune Regulation. *Front Immunol* **9**, 2282 (2018).
36. K. G. Kaval, D. A. Garsin, Ethanolamine Utilization in Bacteria. *mBio* **9**, (2018).
37. S. Shaham, WormBook. *Methods in cell biology*, (2006).
38. L. C. Thomason, N. Costantino, D. L. Court, E. coli Genome Manipulation by P1 Transduction. *Current Protocols in Molecular Biology* **79**, 1.17.11-11.17.18 (2007).
39. T. Baba *et al.*, Construction of Escherichia coli K-12 in-frame, single-gene knockout mutants: the Keio collection. *Mol Syst Biol* **2**, 2006 0008 (2006).
40. P. P. Cherepanov, W. Wackernagel, Gene disruption in Escherichia coli: TcR and KmR cassettes with the option of Flp-catalyzed excision of the antibiotic-resistance determinant. *Gene* **158**, 9-14 (1995).
41. F. Antignano, S. C. Mullaly, K. Burrows, C. Zaph, Trichuris muris infection: a model of type 2 immunity and inflammation in the gut. *J Vis Exp*, (2011).
42. I. Irnov *et al.*, Crosstalk between the tricarboxylic acid cycle and peptidoglycan synthesis in Caulobacter crescentus through the homeostatic control of alpha-ketoglutarate. *PLoS Genet* **13**, e1006978 (2017).
43. M. E. Pacold *et al.*, A PHGDH inhibitor reveals coordination of serine synthesis and one-carbon unit fate. *Nat Chem Biol* **12**, 452-458 (2016).
44. W. W. Chen, E. Freinkman, T. Wang, K. Birsoy, D. M. Sabatini, Absolute Quantification of Matrix Metabolites Reveals the Dynamics of Mitochondrial Metabolism. *Cell* **166**, 1324-1337 e1311 (2016).
45. Y. Simon-Manso *et al.*, Metabolite profiling of a NIST Standard Reference Material for human plasma (SRM 1950): GC-MS, LC-MS, NMR, and clinical laboratory analyses, libraries, and web-based resources. *Anal Chem* **85**, 11725-11731 (2013).

369 46. C. A. Smith *et al.*, METLIN: a metabolite mass spectral database. *Ther Drug*
370 *Monit* **27**, 747-751 (2005).
371 47. P. Virtanen *et al.*, SciPy 1.0: fundamental algorithms for scientific computing in
372 Python. *Nat Methods* **17**, 261-272 (2020).
373 48. R. Kolde. (2015).
374 49. M. I. Love, W. Huber, S. Anders, Moderated estimation of fold change and
375 dispersion for RNA-seq data with DESeq2. *Genome Biol* **15**, 550 (2014).
376 50. P. K. Martin *et al.*, Autophagy proteins suppress protective type I interferon
377 signalling in response to the murine gut microbiota. *Nat Microbiol* **3**, 1131-1141
378 (2018).

Acknowledgements

We wish to thank D. Jones, R. Rose, and L. Ash from the NYU Langone Health Metabolomics Laboratory (SCR_017935; funded by P30CA016087) and C. Yun, S. Cook, and D. Kahler from the High Throughput Biology Core for their help in acquiring and analyzing the data presented. We also thank H. Darwin for advice on microbial metabolism; S. Marion, C. Linton, M. Xu, A. Niranjan, D. Stokes, M. Lopez-Redondo, I. Irnov, V. Torres, S. Dyzenhaus, M. Hui, J. Richards (NYU), P. Loke, J. Lin (NIH), L. Webb, and E. Tait Wojno (Univ. of Washington) for technical assistance and reagents; members of the Hubbard and Cadwell Labs and NYU Medical Scientist Training Program for constructive comments; and M. Alva, J. Carrasquillo, and D. Basnight for assistance with gnotobiotics. Figures 2A, 2K, 3A, 3C, and 4A were created using BioRender.com.

Funding

NIH grant DK093668 (K.C.)
NIH grant AI121244 (K.C.)
NIH grant HL123340 (K.C.)
NIH grant AI130945 (K.C.)
NIH grant AI140754 (K.C.)
NIH grant DK124336 (K.C.)
NIH grant R01GM130152 (E.J.A.H.)
NIH grant R35GM134876 (E.J.A.H.)
NIH grant 5T32AI100853 (M.V.)
NIH grant GM126573 (M.V.)
Faculty Scholar grant from the Howard Hughes Medical Institute (K.C.)
Crohn's & Colitis Foundation (K.C.)
Kenneth Rainin Foundation (K.C.)
Judith & Stewart Colton Center of Autoimmunity (K.C.)
US National Cancer Institute (CA217809) (E.T.K.)
K.C. is a Burroughs Wellcome Fund Investigator in the Pathogenesis of Infectious Diseases.

Author contributions

M.V., R.D., E.J.A.H, and K.C. conceived the study and designed the experiments. M.V. and R.D. performed, analyzed, and interpreted all the experiments for *T. muris* and *C. elegans*, respectively. D.J.L. performed the bacterial cloning. H.S.P and E.T.K provided DarkZone and technical advice. K.C., E.J.A.H, and J.G.B oversaw analysis and interpretation of all experiments described. M.V., R.D., E.J.A.H., and K.C. wrote the manuscript with inputs from all authors.

Competing interests

K.C. has received research support from Pfizer, Takeda, Pacific Biosciences, Genentech, and Abbvie. K.C. has consulted for or received honoraria from Puretech Health, Genentech, and Abbvie. K.C. holds U.S. patent 10,722,600 and provisional patent 62/935,035 and 63/157,225, and E.J.A.H. holds US patent 6,087,153.

Data and materials availability

All data needed to evaluate the conclusions in this study are available in the main text and the supplementary materials or available from the corresponding authors upon request.

Supplementary Materials

Materials and Methods

Figs. S1 to S7

Tables S1-S5

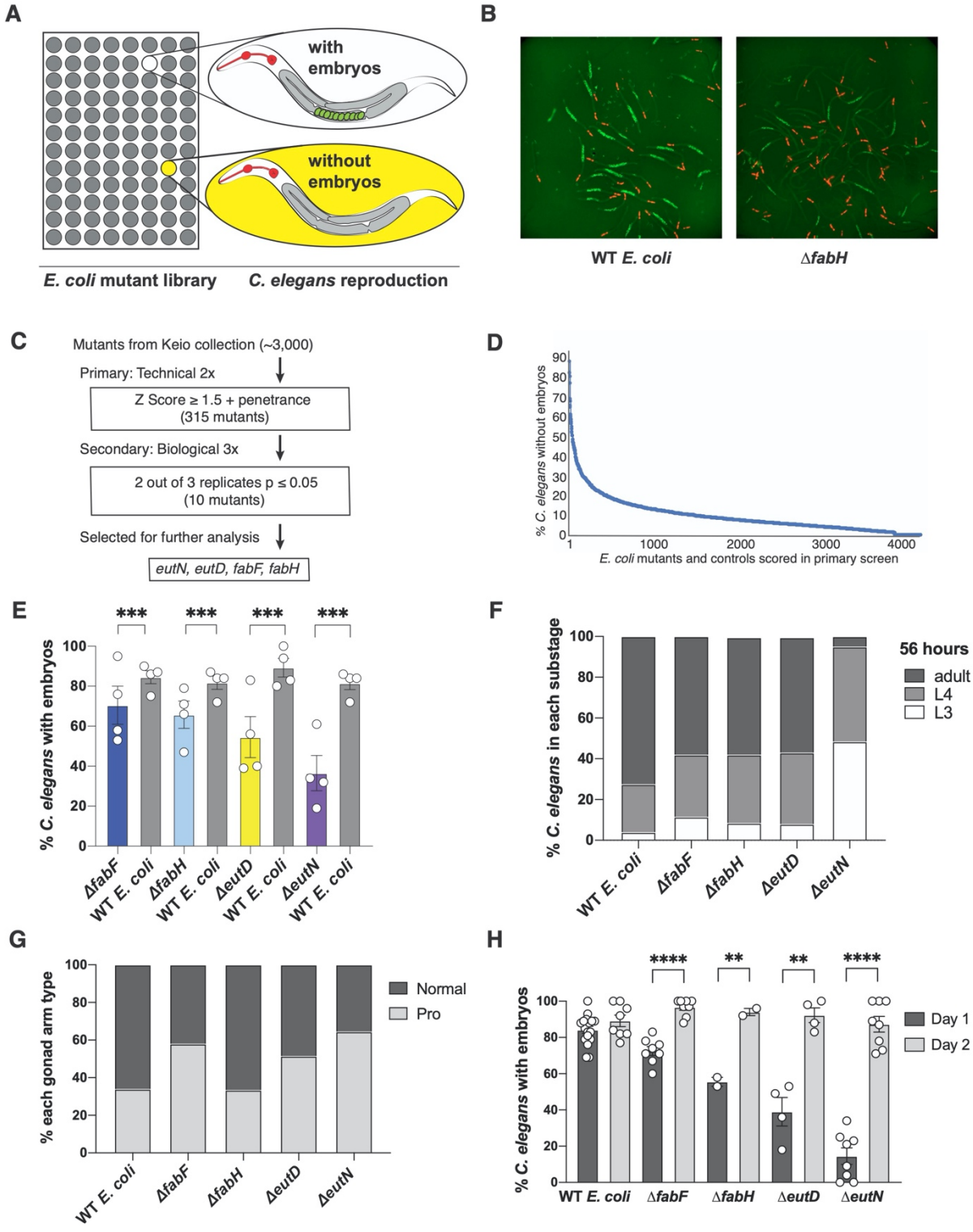

Fig. 1 Identification of *E. coli* mutants that delay *C. elegans* fertility. (A) Concept of high throughput screening of *C. elegans* raised on *E. coli* mutants from the Keio library.

(B) Example of reduced penetrance of *C. elegans* bearing embryos at a single time-point; embryos marked with GFP and pharynx with mCherry. **(C)** Detailed flowchart for schematic in (A). **(D)** Raw primary screen results recorded as percentage of worms without embryos in each well. **(E)** Percentage of *C. elegans* bearing embryos in replicates of four *E. coli* mutants of interest from the screen. In each case, $p \leq 0.001$ for each mutant versus its control from the same plates; total n number of worms scored are (left to right): 409, 923, 242, 387, 189, 522, 163, 501. **(F)** Somatic development is delayed in *C. elegans* raised on *ΔeutN*. Percent of worms at indicated stage at 56 hours after L1 seeding to wells containing the control or mutant bacteria. $n \geq 38$ worms were scored for each *E. coli* mutant. *ΔeutN* is the only mutant that is statistically significantly different from the control GC1547 ($p \leq 0.001$). n number of worms scored (left to right): 52, 59, 61, 40, 54. **(G)** *ΔeutN* and *ΔfabF* delay germline development relative to somatic development. Percent of gonad arms displaying characteristic Pro phenotype. $p \leq 0.001$ for *ΔeutN* and *ΔfabF*. Pooled from two independent trials; n number of worms scored are (left to right): 87, 103, 79, 41, 61. **(H)** Fertility is delayed. Percent of worms with embryos on Day 1 and Day 2. $p \geq 0.05$ (not significant) for any mutant versus the control on Day 2. n number of worms scored (left to right): 547, 297, 242, 242, 60, 46, 124, 121, 253, 261. (D, G) Circles represent mean of each of independent biological replicate and bar is SEM; pairwise Fisher's exact test versus controls (D-F) or Day 1 versus Day 2 (G). ** $p < 0.01$, *** $p < 0.001$, **** $p < 0.0001$.

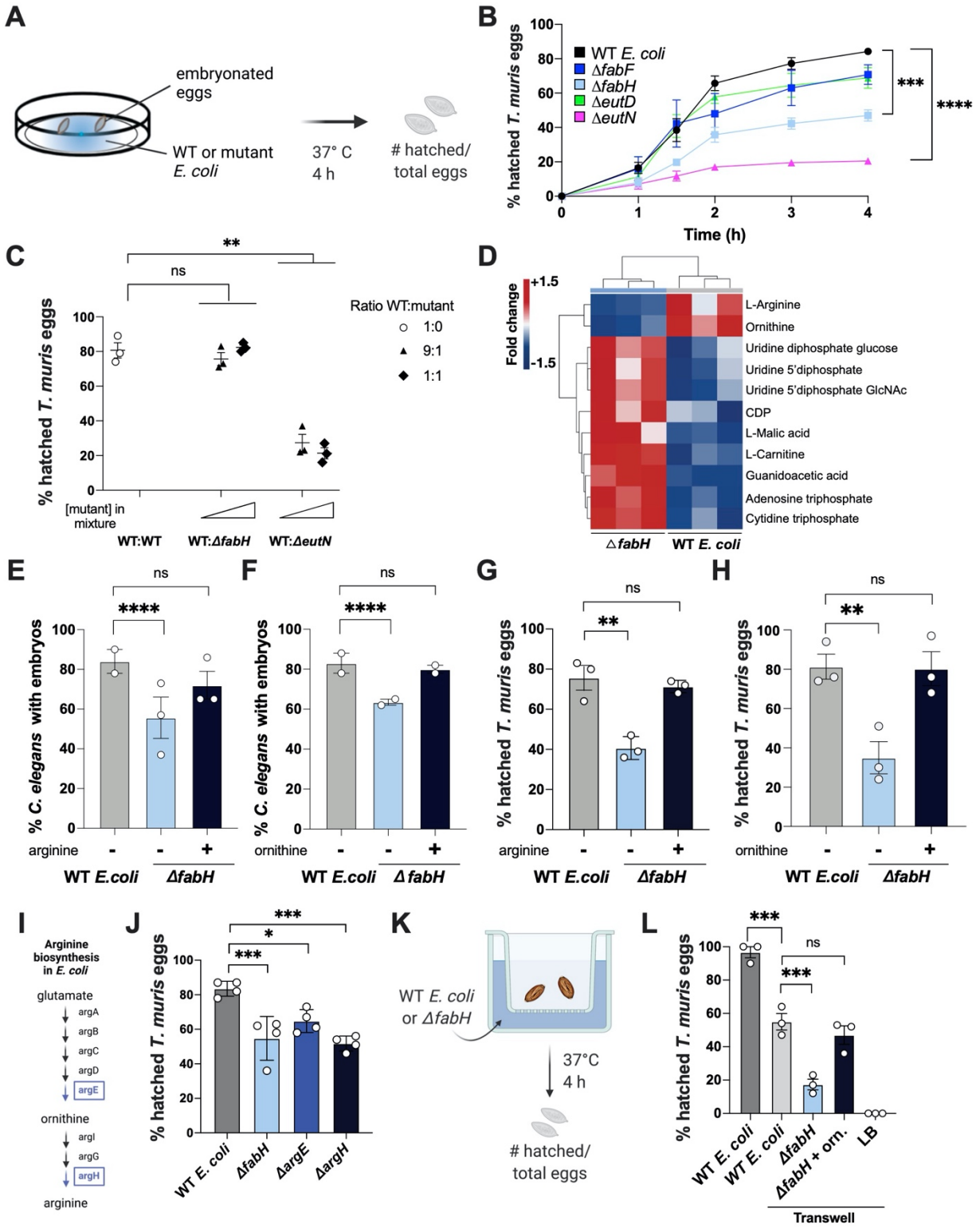

455

456 **Fig. 2 *E. coli* mutants with altered metabolic byproducts delay *C. elegans* fertility**

457 **and inhibit *T. muris* egg hatching. (A)** Experimental approach for *in vitro* hatching

458 assay. **(B)** Percent *in vitro* hatched *T. muris* eggs after incubation with overnight
459 cultures of four *E. coli* mutants identified from the *C. elegans* screen or WT *E. coli*.
460 Hatched eggs were checked using light microscopy at timepoints indicated (n = 4); h =
461 hours. **(C)** Hatching rates for mixtures of WT *E. coli* and either Δ*fabH* or Δ*eutN* overnight
462 cultures in the ratios indicated. Total concentration of each mixture was maintained at
463 1x 10^8 CFU/mL (n = 3). **(D)** Hierarchical clustering of metabolites that were significantly
464 ($p < 0.05$, Student's t-test) downregulated (blue) or upregulated (red) in Δ*fabH* relative to
465 WT. **(E, F)** Percentage of *C. elegans* Day 1 adults with embryos raised on Δ*fabH E. coli*
466 with arginine or ornithine supplementation. Fisher's exact test for Δ*fabH* alone or with
467 supplementation with 500μM arginine or 100μM ornithine compared to WT; Total n
468 number of worms scored (left to right): **(E)** 208, 237, 300 and **(F)** 207, 216, 149. **(G, H)**
469 Percent *in vitro* hatched *T. muris* eggs elicited by Δ*fabH* and cultures supplemented with
470 (G) 500μM arginine or (H) 70μM ornithine where indicated (n=3). **(I)** Arginine
471 biosynthesis pathway in *E. coli*. **(J)** Hatching rates for Δ*argE* and Δ*arg*H (n = 4). **(K)**
472 Experimental approach for hatching assay in a transwell system. **(L)** Hatching quantified
473 for eggs contained within a transwell chamber separated from bacterial culture in the
474 outer chamber by a membrane with 0.4μm pores. Samples supplemented with ornithine
475 as in H are indicated (n = 3). (B) One-way analysis of variance (ANOVA) of area under
476 curve compared to WT. (C, G-H, J, L) One-way analysis of variance (ANOVA) with
477 Dunnett's post-test compared to WT. For all panels, measurements were taken from
478 distinct samples. Graphs show means and SEM. * $p < 0.05$, ** $p < 0.01$, *** $p < 0.001$,
479 **** $p < 0.0001$. ns = not significant.

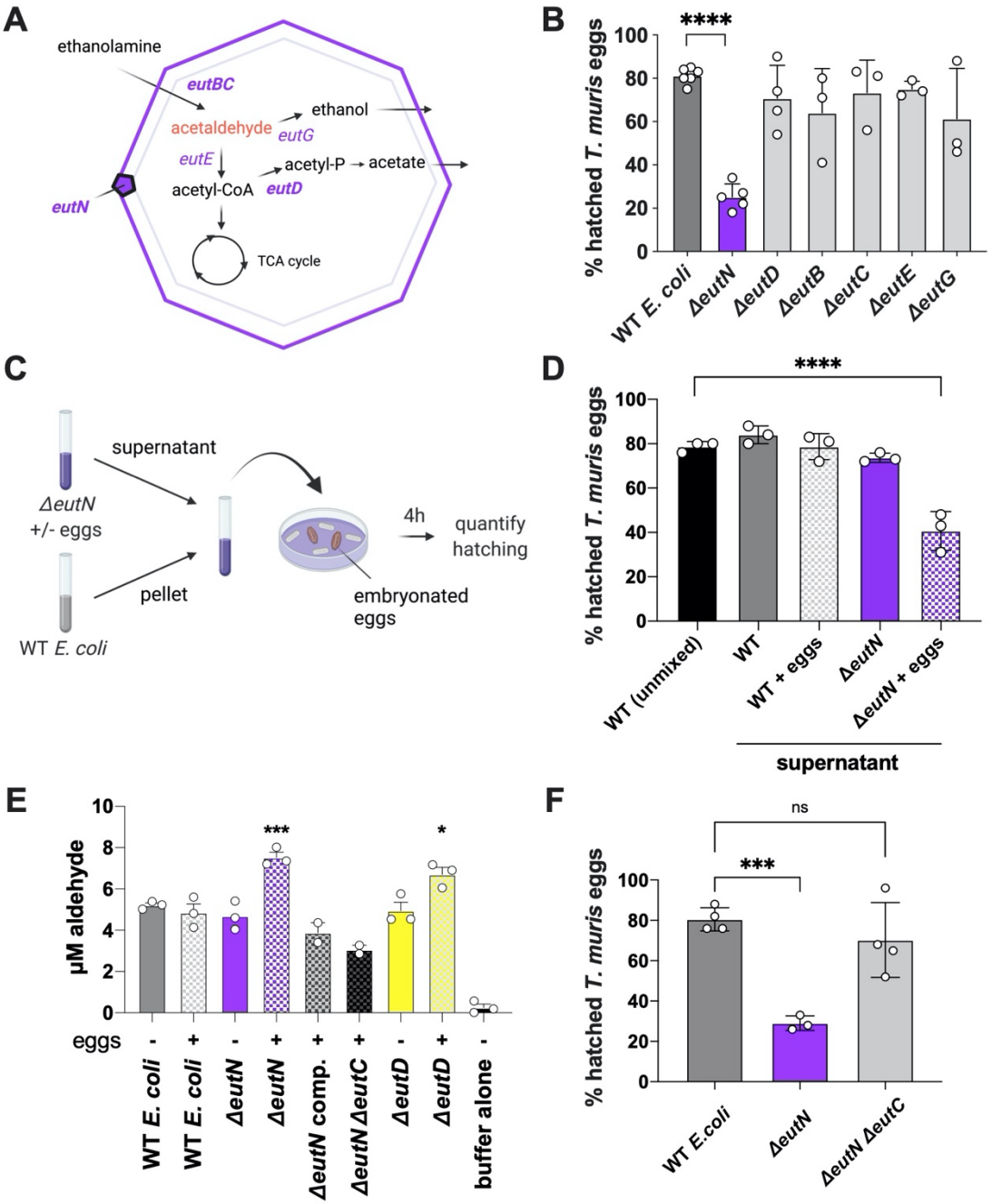

480

481 **Fig. 3 Toxic intermediates of the *E. coli* ethanolamine utilization pathway inhibit *T.***
482 ***muris* egg hatching. (A)** Ethanolamine utilization pathway in *E. coli*. Modified from
483 (*36*). **(B)** Hatching rates for *eut* mutants in the Keio library and WT controls (n = 3-6). **(C)**
484 Experimental approach to assess the toxicity of soluble factors produced by *E. coli*
485 Δ*eutN*. Filtered supernatant from Δ*eutN E. coli* or controls grown with or without *T. muris*
486 eggs for four hours were transferred to a dish containing WT *E. coli* and *T. muris* eggs.

The ability of WT *E. coli* to mediate egg hatching in the presence of supernatant was examined four hours later. **(D)** Quantification of hatching rates in mixtures containing WT *E. coli* cells and the indicated filtered supernatants (n = 3). **(E)** Aldehyde concentrations in supernatants of indicated *E. coli* strains incubated with or without *T. muris* eggs; Δ*eutN* comp. = Δ*eutN* strain where *eutN* has been complemented on a plasmid. **(F)** Hatching rates for Δ*eutN*Δ*eutC* double mutant (n = 4). (B, D-F) Measurements were taken from distinct samples. The average per independent experiment for three technical replicates shown. Graphs show means and SEM. One-way analysis of variance (ANOVA) with Dunnett's post-test compared to WT. * $p < 0.05$, *** $p < 0.001$, **** $p < 0.0001$. ns = not significant.

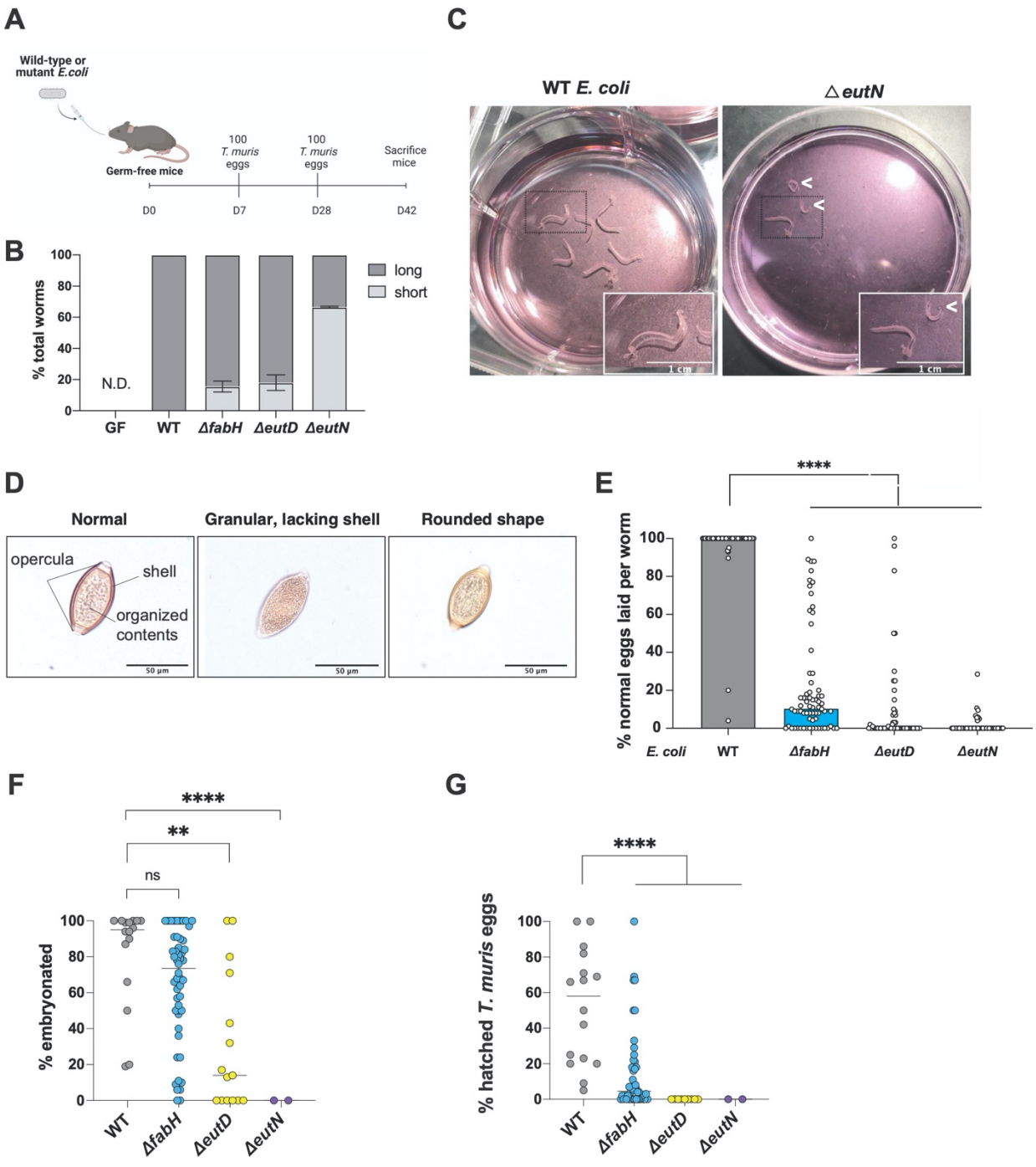

497

498 **Fig. 4 *T. muris* infection of mice colonized with *E. coli* mutants leads to defects in**
499 **worm morphology and fertility. (A)** Experimental approach for *T. muris* infection of
500 mice monocolonized with WT or mutant *E. coli*. **(B)** Proportion of short and long worms
501 harvested per mouse colonized by indicated *E. coli* strains; N.D. = not detected (n = 6-9

mice per group). **(C)** Representative images of worms harvested from mice monocolonized with WT or *ΔeutN E. coli*. A representative short worm (indicated by arrowhead) next to a long worm is shown in the inset for *ΔeutN E. coli*. **(D)** Representative images of eggs laid by worms from (B). Worms were incubated in RPMI medium overnight to trigger egg laying. **(E)** Proportion of total eggs laid per worm with normal morphology. Circles represent individual worms (WT, n = 46; *ΔfabH*, n = 68; *ΔeutD*, n = 58; *ΔeutN*, n = 50). **(F)** Percentage of embryonated eggs following 8-week incubation. **(G)** Percentage of eggs in (F) that hatched after incubation with WT *E. coli* for 4 hours at 37°C. (B, E, F-G) Measurements were taken from distinct samples. Data shown are pooled from two independent experiments. Graphs show (B) means and SEM or (E, F-G) medians. One-way analysis of variance (ANOVA) with Dunnett's post-test compared to WT. ** $p < 0.01$, **** $p < 0.0001$. ns = not significant.

Supplementary Materials

Materials and Methods

Keio Library growth and culture

The frozen Keio collection was stamped out onto 150mm LB kanamycin (30µg/ml) plates and grown overnight at 37°C. For *C. elegans* experiments, individual colonies were inoculated into 700 µl of LB-Kan (30µg/ml) in 96 deep well plates using a compatible pin replicator. The plates were sealed with pure link air porous tape (Invitrogen cat no. 12262010) and incubated for 16-18 hours at 37°C, shaking at 250 rpm. Cultures were diluted 10X in S-media in 96 well format and OD at 600 nm was recorded for future reference to ensure that candidate positive mutants grew to an OD similar to the GC1547 wild-type control wells in the same plate. (This was done since poor bacterial growth can reduce the percentage of gravid *C. elegans*; all 315 candidates from the primary screen passed this control). Bacterial cultures were pelleted by centrifugation at 2000 rpm for 30 minutes. Supernatant was discarded and the pellet was resuspended in 100µl of S-media. 40µl of the culture was transferred into two separate plates (two technical replicates; black-walled, clear bottom 96-well microplates; Corning Cat. No. 3904) using a multi-channel pipette. The GC1547 control wild-type strain was a kanamycin resistant transformant of the Keio library starting strain BW25113, carrying the pET28a plasmid. For *T. muris in vitro* hatching assays, *E. coli* was grown overnight for 12-14 hours in Luria-Bertani broth with shaking at 225 rpm at 37 °C.

Primary screen

C. elegans GC1474 (Table S1; derived by outcrossing GC1373 (*23*) of the genotype *glp-1(e2141); end-1::gfp; myo-2p::mCherry*) was maintained on OP50 *E. coli* on NGM plates at 20ºC and synchronized in the L1 larval stage using hypochlorite treatment followed by overnight hatching in egg buffer (*37*). 40-50 L1 larvae were seeded into 96-well plates in technical duplicate with 40µl of *E. coli* mutant cultures and incubated at

20°C with mild shaking in a humidified chamber for 62-65 hours. At this timepoint, control worms were fully gravid adults; control GC1547 bacteria were included on each plate in wells void of library bacteria. Prior to imaging, 40µl of 2mM levamisole was added to each well to immobilize the worms. The plates were then sealed with aluminum foil (Corning Cat. No. 6570) and imaged to detect both green (embryos) and red (pharynx) fluorescent markers using arrayscan (Thermo Scientific VTI). Images were captured at 2.5X magnification 2x2 binning in a 16 mm^2 field and digitally archived. Images captured on the red and green channels were merged in ImageJ using macros written to automate the process. Each adult animal was scored visually as "with embryos" (green embryos visible in the uterus) or "without embryos" (no green embryos visible in the uterus), and the number of worms without embryos and the total number of worms (excluding any that were arrested or any that crossed the edge of the well). Wells in which many animals had not reached adulthood were marked and were not considered further in our analysis. Ten such bacterial mutants grew well by OD but did not support worm development.

Additional culling of potential hits was performed. A variety of technical factors eliminated fewer than 10% of the total: 54 library wells were devoid of bacteria as per the plate map; 58 had a gene name in the library but the bacteria did not grow (either on solid or liquid culture); 41 were missed due to human error while scoring (noted as largely fertile but not counted individually); 5 had low n; 4 were not included due to reasons classified as 'other' (e.g., poor image) and 10 wells had poor worm growth in both replicates.

Worm counts (with/without embryos) were exported into ActivityBase (IDBS, https://www.idbs.com; a Scientific informatics software platform) and the robust Z score (a statistical measure that takes into account the median plate "without embryos" percent) was calculated for every well to minimize problems associated with plate to plate variation. Each well was analyzed with respect to percent worms without embryos, consistency (across technical replicates) and robust Z score. A cut-off of robust $Z \geq 1.5$ was selected as "Z positive" (≤ 10% of the wells per plate scored above this threshold).

We also calculated the penetrance of worms without embryos for pooled technical replicates.

Criteria for selection in the primary screen weighed the robust Z and penetrance, with special consideration for cases where only one replicate was available. We included those wells for which only one technical replicate was available provided that well made the RobZ cut off (≥ 1.5) and/or percent non-gravid worms as further described below. Reasons for single-replicate included low n (62 wells), human error (49 wells), worm arrest (31 wells), poor image quality (22 wells) and 1 well marked as 'other'. Considering Z score, penetrance and replicates, the candidates were further classified as follows: High, A: both replicates Z positive and average penetrance of non-gravid worms > 20%, or B: one replicate available and it is Z positive and > 20%, or C: both replicates available but only one is Z positive and non-gravid ≥ 30%. Medium, A: both replicates Z positive and pooled non-gravid percent 13-20%, or B: only one replicate available which is Z positive and 13-20% penetrance of worms without embryos, or C: both replicates available but only one is Z positive with pooled non-gravid penetrance between 20-30%. Low: both replicates available, but only one is Z positive and non-gravid percent between 12.5-20%. This analysis yielded 315 primary screen candidates.

We then plotted the percent non-gravid in descending order for every well per plate and noted the inflection point (see (*23*)). We placed a subset of the mutants that passed the criteria above onto these plots and observed a strong correlation: wells with larger Z scores all appeared above the inflection point.

Secondary screen: reproducibility

The 315 candidates from the primary screen were re-selected from the original Keio library and gridded onto secondary screen plates. Two plates included only high priority candidates or a combination of randomly selected high, medium and low priority candidates to help assess whether there was a correlation between penetrance and reproducibility. No such correlation emerged, but these plates were considered as additional replicates in the analysis going forward (hence 6 plates) though 315 mutants.

Control bacteria were included in all secondary screen plates. Three biological replicates were performed in technical triplicate and scored and analyzed as described above. Technical replicate non-gravid/gravid counts were pooled and analyzed in pairwise comparison with the control on the same plates using Fisher's exact test. Candidates with p-values ≤ 0.05 in at least 2 out of 3 biological replicates were chosen for further analysis. This analysis yielded 10 candidates.

PCR validation of selected Keio mutants (completed for all ten hits)

We amplified and sequenced PCR fragments ~150 bp upstream and downstream of the predicted gene from each mutant and the control. Nested primers were used to sequence the PCR fragment and confirm the presence of the FRT and kanamycin cassette in the mutant DNA (Tables S3, S5).

P1 transduction

Mutant alleles comprising a kanamycin-resistance marker within a gene deletion were introduced into BW25113 by P1 transduction (*38*) from the Keio collection (*39*) .The kanamycin-resistance cassette was subsequently excised to generate a markerless in-frame gene deletion by transformation with the temperature-sensitive plasmid pCP20 (*40*), which encodes FLP recombinase, and growth at 30°C. Finally, pCP20 was eliminated from the cells by growth at 42°C.

Complementation

For *fabH* and *eutN*, the bacterial gene coding regions plus 20 bp upstream were inserted into pBR322 downstream of a plasmid promoter by Gibson Assembly. The wild-type genomic DNA was amplified and assembled with a PCR fragment obtained from the pBR322 vector (specific primers are listed in Table S3; the fragment excluded part of the Amp^R gene between *Eco*RI and *Pst*I restriction site). PCR products were purified using gel extraction kit (QIAEX II cat no. 20021) and 100 ng of vector was used

637 in 1:1 molar reaction with the genomic fragment. The assembly reaction was then
638 transformed into high efficiency DH5alpha cells (NEB C2987I). Plasmid preparations
639 (Qiagen mini prep kit Cat no.27106) were sequenced using pBR322 specific primers
640 (Table S4). Plasmids were confirmed by DNA sequence and transformed into the
641 respective mutant (named as strains GC1558 and GC1559 for *eutN* rescue and *fabH*
642 rescue, respectively) and tested for reduced penetrance of the *C. elegans* non-gravid
643 phenotype upon feeding.
644
645 **Developmental timing and germline analysis**
646
647 *Somatic development assay*
648 *C. elegans* were maintained on OP50, synchronized by hypochlorite treatment and
649 allowed to hatch at 20ºC with shaking. 30-40 L1 larvae were seeded in 96 deep well
650 plates with each well carrying a specific mutant clone. Worms were incubated at 20ºC
651 with shaking for 48 hours and monitored at 400X on a Zeiss Z1 Axio Imager for vulval
652 morphology (*24*) at specific time points.
653
654 *Pro phenotype assay*
655 *glp-1(ar202)* animals were scored for the Pro phenotype upon feeding with mutant
656 bacteria using the same strategy as for the primary screen. Worms were maintained at
657 15ºC on OP50 synchronized and grown in 96 deep well format as above. Day 1 (~72
658 hours post seeding) worms were fixed and DAPI stained and each gonad arm was
659 scored for the Pro phenotype (*25*) at 400X.
660
661 *Fertility at Day 2*
662 GC1474 worms were maintained at 20ºC on OP50, synchronized as L1 larvae and
663 grown in 96 deep well format as above. Worms were anesthetized and imaged as in the
664 screen on Day 1 and Day 2 to determine changes in penetrance of fertile worms.
665
666 *Progenitor zone nuclei counts at L4-Adult molt*

Worms grown on GC1547 control, *eutN*, *eutD,* and *fabH* mutant bacteria were monitored for vulval development and isolated at the L4-adult molt. Worms were then stained with DAPI (*22*) and 0.5µm Z-stack images were collected and analyzed using ImageJ to determine the number of germ cells in the PZ. In approximately 30% of the worms, the transition zone was not clear. These were censored from the analysis.

Assay for dependence on DAF-7/TGFß and DAF-2 IIS pathways

C. elegans strains GC1474, GC1545 and GC1250 (Table S2) were hypochlorite-synchronized and hatched overnight at 20ºC. L1 larvae were seeded into 96 deep well plates containing specific bacterial mutants and scored for the presence of embryos in adults on Day 1 on Zeiss compound microscope at 100X.

Parasite maintenance

Stock eggs of *T. muris* E strain (*7*) were maintained in the NOD.Cg-*Prkdc*^{scid}/J (Jax) mouse strain in a specific pathogen free (SPF) facility and propagated as previously described (*41*). Each egg batch was confirmed to hatch at ≥ 80% *in vitro* using method below and WT *E. coli* before use in subsequent experiments.

***In vitro* hatching of *T. muris* eggs**

T. muris eggs were hatched *in vitro* by mixing 25µL of embryonated eggs at a concentration of 1 egg/1µL suspended in sterile water with 10µL of *E. coli* overnight culture and 15µL sterile LB in individual wells of a 48 well plate. Plates were incubated at 37°C and checked every hour for a total of four hours on the Zeiss Primovert microscope to enumerate hatched eggs. Rates describe hatching after four hours of incubation unless otherwise indicated. Experiments utilizing transwell inserts (Millicell) were performed as previously described (*5*). For experiments where cell-free supernatant was used, supernatant and cells were isolated by centrifugation and filtration through a 0.22µm syringe filter or after wash with autoclaved ddH20,

respectively. Incubation with embryonated eggs was performed by mixing *T. muris* eggs at a concentration of 15 eggs/2 mL culture and keeping at 37°C for four hours.

Metabolomics

Sample preparation

Individual colonies (obtained after streaking frozen bacteria onto LB-kanamycin plates and incubating at 37ºC) were inoculated in 30 ml of LB-kanamycin (30µg/ml) liquid in a 50ml falcon tube. Cultures were grown for 16-18hr at 37ºC with 250 rpm shaking and then bacteria were pelleted by centrifugation at 1500 rpm for 20-30 minutes at 4ºC. The supernatant was transferred to a fresh tube, filtered through 0.2µm filter (Corning (431229) and frozen at -80ºC for future analysis. Pellets were resuspended in 7.5 ml of S-media (for ~250ml of S-media the recipe was 240ml of S-basal, 2.5ml of 1M potassium citrate- final concentration of 10mM, 2.5ml of 1M trace metals for final concentration of 10mM, 750µl of 1M $MgS0_4$ for final concentration of 3mM, 750µl of 1M $CaCl_2$ for final concentration of 3mM, 72µl of 100mg/ml of kanamycin for final concentration of 30µg/ml). This solution was filter sterilized using a 500ml Nalgene filter (291-3320 Fisher). Post filter sterilization, 250µl of 5mg/ml cholesterol – final concentration of 5µg/ml and 2.5ml of 250µg/ml fungizone for final concentration of 2.5µg/ml (BP264550 Fisher).

The number of CFU/ml was estimated for each culture by plating dilutions (10µl of culture was mixed with 900µl of S-media to get 10^2 or 1:100 dilution, which was then serially diluted to 1:10^5 or 1:10^6 on LB agar plates and counting colonies after growth at 37°C. The remaining culture was incubated at 20ºC with mild shaking overnight to mimic *C. elegans* growth conditions. Based on CFU/ml measurements, 10^{10} cells were fast filtered (EZFIT Vacuum Manifold, Millipore EZFITLOW03 with Microfil V, Millipore MVHAWG124) and metabolite extracts were isolated as previously described (*42*). Three independent biological samples were extracted on three independent days and subsequently analyzed by the NYU Langone Metabolomics Core Resource Library.

LC-MS/MS with the hybrid metabolomics method

Samples were subjected to an LCMS analysis to detect and quantify known peaks. A metabolite extraction was carried out on each sample based on a previously described method (*43*). The LC column was a Millipore^{TM} ZIC-pHILIC (2.1 x150mm, 5µm) coupled to a Dionex Ultimate 3000^{TM} system and the column oven temperature was set to 25^{o}C for the gradient elution. A flow rate of 100µL/min was used with the following buffers: A) 10mM ammonium carbonate in water, pH 9.0, and B) neat acetonitrile. The gradient profile was as follows; 80-20%B (0-30 min), 20-80%B (30-31 min), 80-80%B (31-42 min). Injection volume was set to 2µL for all analyses (42 min total run time per injection).

MS analyses were carried out by coupling the LC system to a Thermo Q Exactive HF^{TM} mass spectrometer operating in heated electrospray ionization mode (HESI). Method duration was 30 min with a polarity switching data-dependent Top 5 method for both positive and negative modes. Spray voltage for both positive and negative modes was 3.5kV and capillary temperature was set to 320^{o}C with a sheath gas rate of 35, aux gas of 10, and max spray current of 100µA. The full MS scan for both polarities utilized 120,000 resolution with an AGC target of 3e6 and a maximum IT of 100ms, and the scan range was from 67-1000 *m*/*z*. Tandem MS spectra for both positive and negative mode used a resolution of 15,000, AGC target of 1e5, maximum IT of 50ms, isolation window of 0.4m/z, isolation offset of 0.1m/z, fixed first mass of 50m/z, and 3-way multiplexed normalized collision energies (nCE) of 10, 35, 80. The minimum AGC target was 1e4 with an intensity threshold of 2e5. All data were acquired in profile mode.

Hybrid Metabolomics Data Processing

Relative quantification of metabolites

The resulting Thermo^{TM} RAW files were converted to mzXML format using ReAdW.exe version 4.3.1 to enable peak detection and quantification. The centroided data were searched using an in-house python script Mighty_skeleton version 0.0.2 and peak

753 heights were extracted from the mzXML files based on a previously established library
754 of metabolite retention times and accurate masses adapted from the Whitehead
755 Institute (*44*), and verified with authentic standards and/or high resolution MS/MS
756 spectral manually curated against the NIST14MS/MS (*45*) and METLIN (2017)(*46*)
757 tandem mass spectral libraries. Metabolite peaks were extracted based on the
758 theoretical *m*/*z* of the expected ion type e.g., $[M+H]^+$, with a ±5 part-per-million (ppm)
759 tolerance, and a ± 7.5 second peak apex retention time tolerance within an initial
760 retention time search window of ± 0.5 min across the study samples. The resulting data
761 matrix of metabolite intensities for all samples and blank controls was processed with an
762 in-house statistical pipeline Metabolyze version 1.0 and final peak detection was
763 calculated based on a signal to noise ratio (S/N) of 3X compared to blank controls, with
764 a floor of 10,000 (arbitrary units). For samples where the peak intensity was lower than
765 the blank threshold, metabolites were annotated as not detected, and the threshold
766 value was imputed for any statistical comparisons to enable an estimate of the fold
767 change as applicable. The resulting blank corrected data matrix was then used for all
768 group-wise comparisons, and t-tests were performed with the Python SciPy (1.1.0) (*47*)
769 library to test for differences and generate statistics for downstream analyses. Any
770 metabolite with p-value < 0.05 was considered significantly regulated (up or down).
771 Heatmaps were generated with hierarchical clustering performed on the imputed matrix
772 values utilizing the R library pheatmap (1.0.12) (*48*). Volcano plots were generated
773 utilizing the R library, Manhattanly (0.2.0). In order to adjust for significant covariate
774 effects (as applicable) in the experimental design the R package, DESeq2 (1.24.0) (*49*)
775 was used to test for significant differences. Data processing for this correction required
776 the blank corrected matrix to be imputed with zeroes for non-detected values instead of
777 the blank threshold to avoid false positives. This corrected matrix was then analyzed
778 utilizing DESeq2 to calculate the adjusted p-value in the covariate model.

779 **Arginine and ornithine supplementation assay**

780 *fabH* mutant *E. coli* or wild-type control was grown with arginine (400μM or 500μM) or
781 ornithine (40-100mM) in LB-kanamycin overnight at 37ºC with 250 rpm shaking. For *C.*

elegans experiments, worms were imaged on Day 1 as described for the primary screen. For *T. muris* experiments, hatching assay was performed as described above.

DarkZone labeling of aldehydes

Cell-free supernatants isolated from *E. coli* overnight cultures were incubated with 20μM DarkZone dye pre-dissolved in DMSO, 5mM 2,4 dimethoxyaniline catalyst (TCI America) pre-dissolved in DMSO, and buffer (100mM Tris pH 6.8, 150 mM NaCl) in a 96 well optical flat-bottom plate (Thermo-Fisher) in duplicate at 37°C for 1 hour. Adhesive plate seals were used to prevent evaporation of aldehydes. Fluorescence was measured using an EnVision 2 103 Multi-label Reader (PerkinElmer). Duplicate measurements were averaged.

Mice

Gnotobiotics

Previously described germ-free C57BL/6J mice (*50*) were maintained in flexible film isolators, and absence of faecal bacteria and fungi was confirmed by aerobic culture in brain heart infusion, sabaraud and nutrient broth (Sigma), and qPCR for bacterial 16S and eukaryotic 18S ribosomal RNA genes through sampling of stool from individual cages in each isolator on a monthly basis. Mice were transferred into individually ventilated Tecniplast ISOcages for infections to maintain sterility under positive air pressure. All animal studies were performed according to approved protocols and ethical guidelines established by the NYU Grossman School of Medicine Institutional Animal Care and Use Committee (IACUC) and Institutional Review Board.

Murine in vivo infections

Female mice were monocolonized at 6-8 weeks of age by oral gavage with 1×10^8 colony forming units per mL (CFU/mL) of indicated *E. coli* strains. Overnight *E. coli* cultures were diluted 1:100 in Luria-Bertani broth followed by 2-3 hours of growth until 1×10^8 CFU/mL was reached. Bacterial density was confirmed by dilution plating.

Cultures were pelleted by centrifugation at 2437g for 10 minutes and washed once with sterile 1x PBS. Pellets were then resuspended in sterile 1x PBS and mice were inoculated by oral gavage with $1x10^8$ CFU in a volume of 100µL. Inoculum was verified using dilution plating of aliquots.

7 and 28 days later, mice were infected by oral gavage with ~100 embryonated *T. muris* eggs. Individual worms were collected from cecal contents of all infected mice and washed in RPMI 1640 (Invitrogen) supplemented with penicillin (100U/ml) and streptomycin (100µg/ml; Sigma). To evaluate egg laying, each worm was placed into individual wells of a 48 well plate with 200µL supplemented RPMI. Plates were then incubated at 37°C overnight in a closed tupperware (Sistema) lined with damp paper towels. The following day, eggs laid were enumerated using a Zeiss Primovert light microscope at 100X. Samples containing ~1000 eggs per condition were mounted on glass slides with glycerol mounting medium (Sigma-Aldrich) and analyzed using a Zeiss Axio Observer at 400X with oil emersion for color images or EVOS FL Auto (Life Technologies) at 200X for black and white images. Images were processed using ImageJ.

Statistical analysis

Statistical tests and parameters used, including the definition of central value and the exact number (n) of mice or worms per group, are annotated in the corresponding figure legend. All analyses were performed with Graphpad Prism version 8.4.3 for Mac (GraphPad). The numbers of animals or biological replicates used herein were estimated on the basis of a power analysis with the following assumptions: the standard deviation will be roughly 20% of the mean; *p* values will be less than 0.05 when the null hypothesis is false; and the effect size (Cohen's *d*) is between 1.0 and 2.0. We have also carefully chosen the indicated sample size on the basis of empirical evidence of what is necessary to interpret the data and statistical significance.

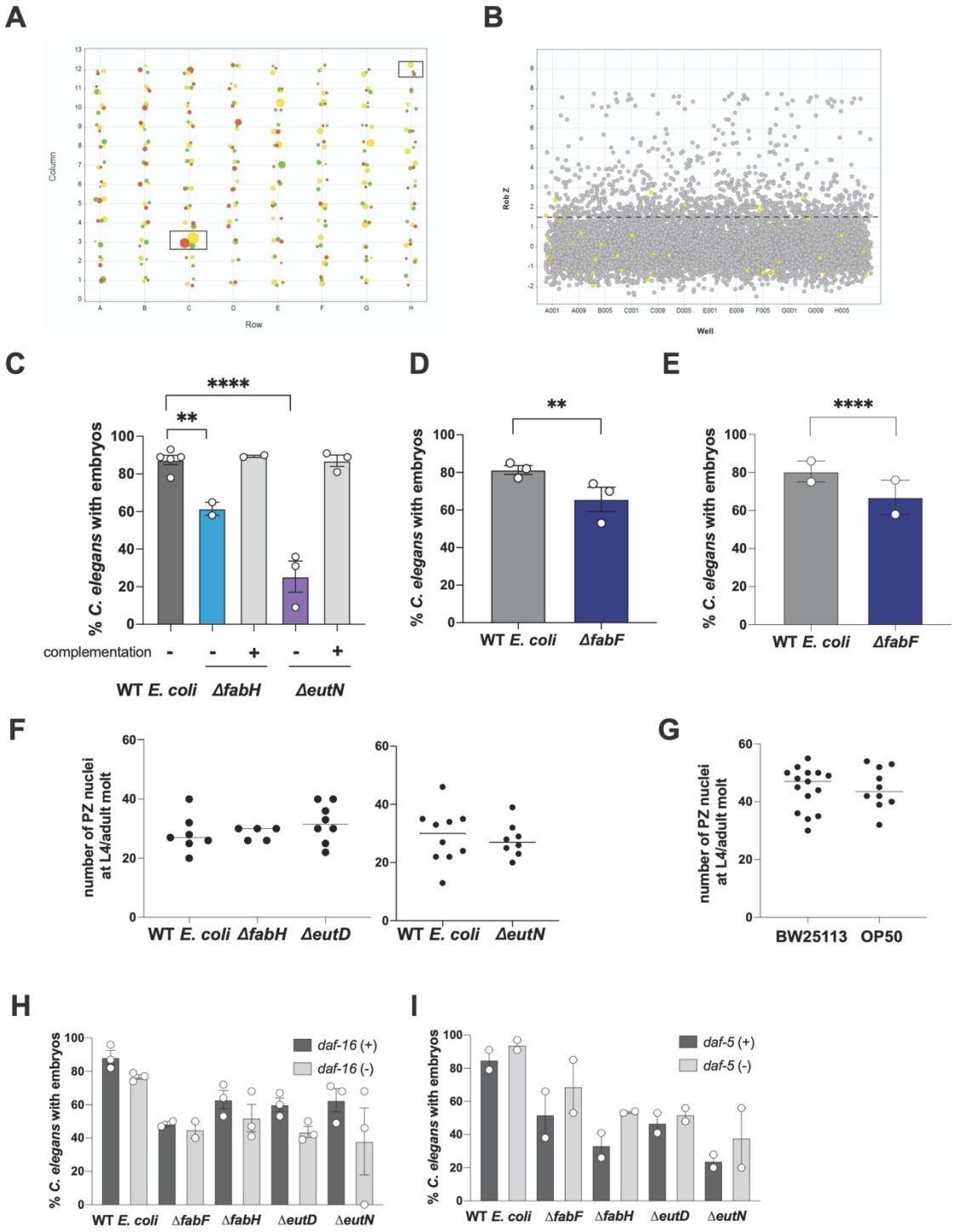

Fig. S1 Primary screen selection criteria, validation of *E. coli* mutants, and effect of mutant *E. coli* on *C. elegans*. (A) Representative bubble plot from secondary screen replicates. One of the six 96-well plates used in the secondary screen is shown here rendered using Vortex software data visualization tool. The size of the bubble

represents percent of worms without embryos that is calculated from three technical replicates, while the color indicates the three biological trials. Boxed wells H12 and C3 indicate the negative control and a positive hit in two out of three replicates based on statistical tests (see Methods)**. (B)** Scatter plot showing the Robust Z (Rob Z) score for all primary screen wells scored. Scatter plot was generated using Vortex dotmatics software. Yellow dots indicate wells containing the negative control bacteria (GC1547). Dashed line indicates cut-off for Rob Z criterion. **(C)** Δ*eutN* and Δ*fabH* complementation suppresses *C. elegans* fertility defect. $p \leq 0.0001$ by Fisher's exact test compared to WT; n total number of worms scored in each case is (left to right): 925, 220, 197, 744, 1078. **(D, E)** Δ*fabF* phage transductants mimic *C. elegans* fertility defect of Δ*fabF* original clone. Circles represent mean of four independent biological replicates and bar is SEM. (D) $p \leq 0.007$ for original *fabF* clone (n = 330, 214 worms scored in WT and Δ*fabF*, respectively), and (E) $p \leq 5x10^{-5}$ (n = 231, 66), Fisher's exact test, compared to control GC1547 bacteria in each case. **(F)** The number of progenitor zone nuclei of *glp-1(e2141)* at the L4 to Adult molt is not altered in worms raised on Δ*eutN*, Δ*fabH* or Δ*eutD* versus wild-type *E. coli*. Scatter plots showing number of progenitor zone germ cell counts; each dot represents one gonad arm. We noted that in ~30% of *eutN* mutants (relative to 10% in control), the border of the PZ was difficult to detect; these were censored from PZ counts. The elevated penetrance of this phenotype in the Δ*eutN*-fed worms may represent a meiotic entry defect, accounting for the delay in germline development relative to somatic development. **(G)** No significant difference is observed between the number of progenitors in worms grown on BW25113 versus OP50 on standard NGM solid media ($p \geq 0.05$, Student's t-test). We note that the number of progenitors is markedly lower in the *glp-1(e2141)* mutant background after growth on liquid versus growth on solid media; the Keio starting strain was used in (G) since OP50 is sensitive to kanamycin. **(H, I)** Fertility delay is not suppressed by loss of *daf-16* or *daf-5*. Percent of worms with embryos on Day 1 in (H) *daf-16(+); daf-2(e1370) glp-1(e2141) or daf-16(m26); daf-2(e1370) glp-1(e2141)* and (I) *daf-5(+); glp-1(e2141) or daf-5(e1386); glp-1(e2141).* Although a significant difference was detected by Fisher's exact test between *daf-5(+)* and *daf-5(-)* for Δ*eutN* ($p < 0.0001$) and Δ*fabH* ($p < 0.0001$), this was not considered biologically meaningful since the *daf-5(e1386)* worms

raised on GC1547 bore significantly more embryos in comparison to the *daf-5(+)* worms raised on the GC1547 control ($p \leq 0.0027$). Circles represent mean of independent biological replicates and bar is SEM. n total number of worms scored are (left to right): **(I)** 269, 203,207, 245, 179, 255, 229, 214, 200, 233 and **(J)** 59, 65, 71, 62, 179, 73, 64, 54, 56, 57.

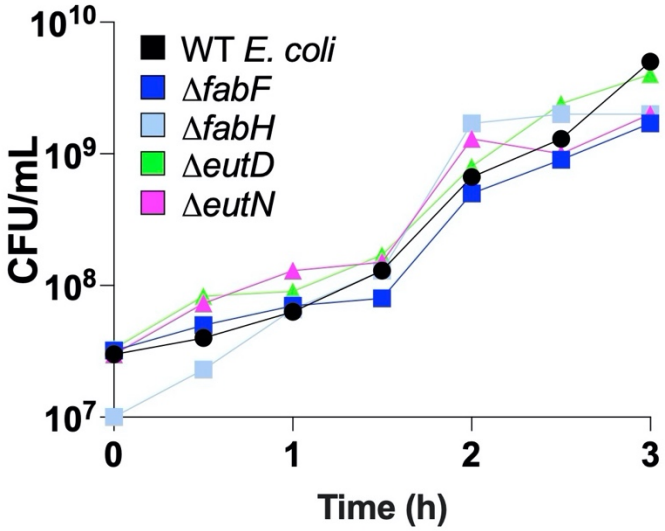

877

878 **Fig. S2 *E. coli* mutants used for *T. muris* egg hatching assay display similar *in***
879 ***vitro* growth kinetics as wild-type bacteria.**

880 Bacterial density of monoclonal cultures of each of the strains indicated measured by
881 dilution plating; CFU = colony forming units, h = hours.

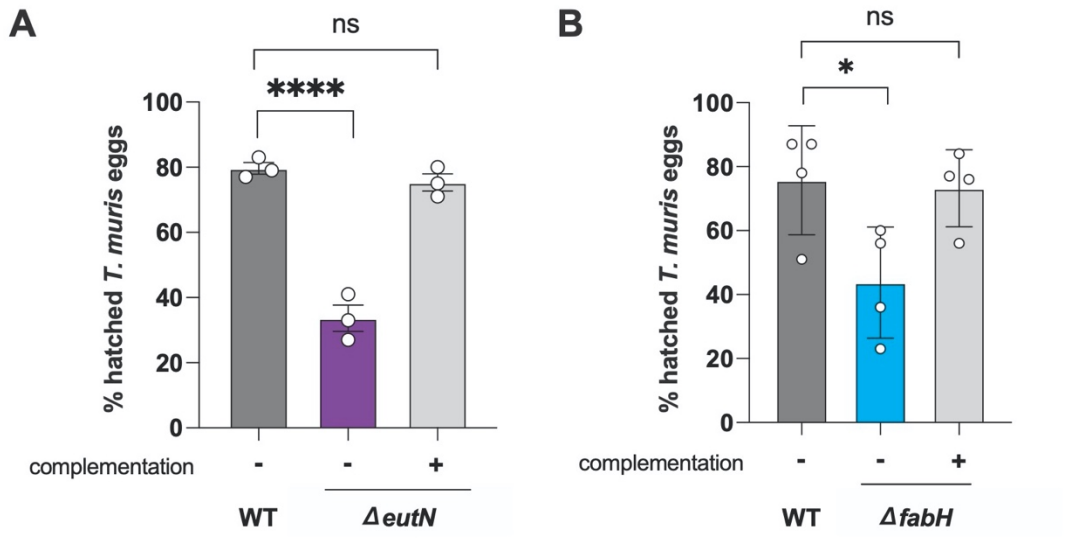

882

883 **Fig. S3 Complementation of Δ*fabH* and Δ*eutN E. coli* rescue *T. muris* egg**
884 **hatching.**

885 Hatching elicited by WT *E. coli* (WT), mutants **(A)** Δ*eutN* and **(B)** Δ*fabH*, and strains
886 where deletions were complemented with a plasmid-borne gene (n = 3-4).
887 Measurements were taken from distinct samples. Data represent the average of at least
888 three independent experiments. Graphs show means and SEM. One-way analysis of
889 variance (ANOVA) with Dunnett's post-test compared with WT. * $p < 0.05$, **** $p <$
890 0.0001. ns = not significant.

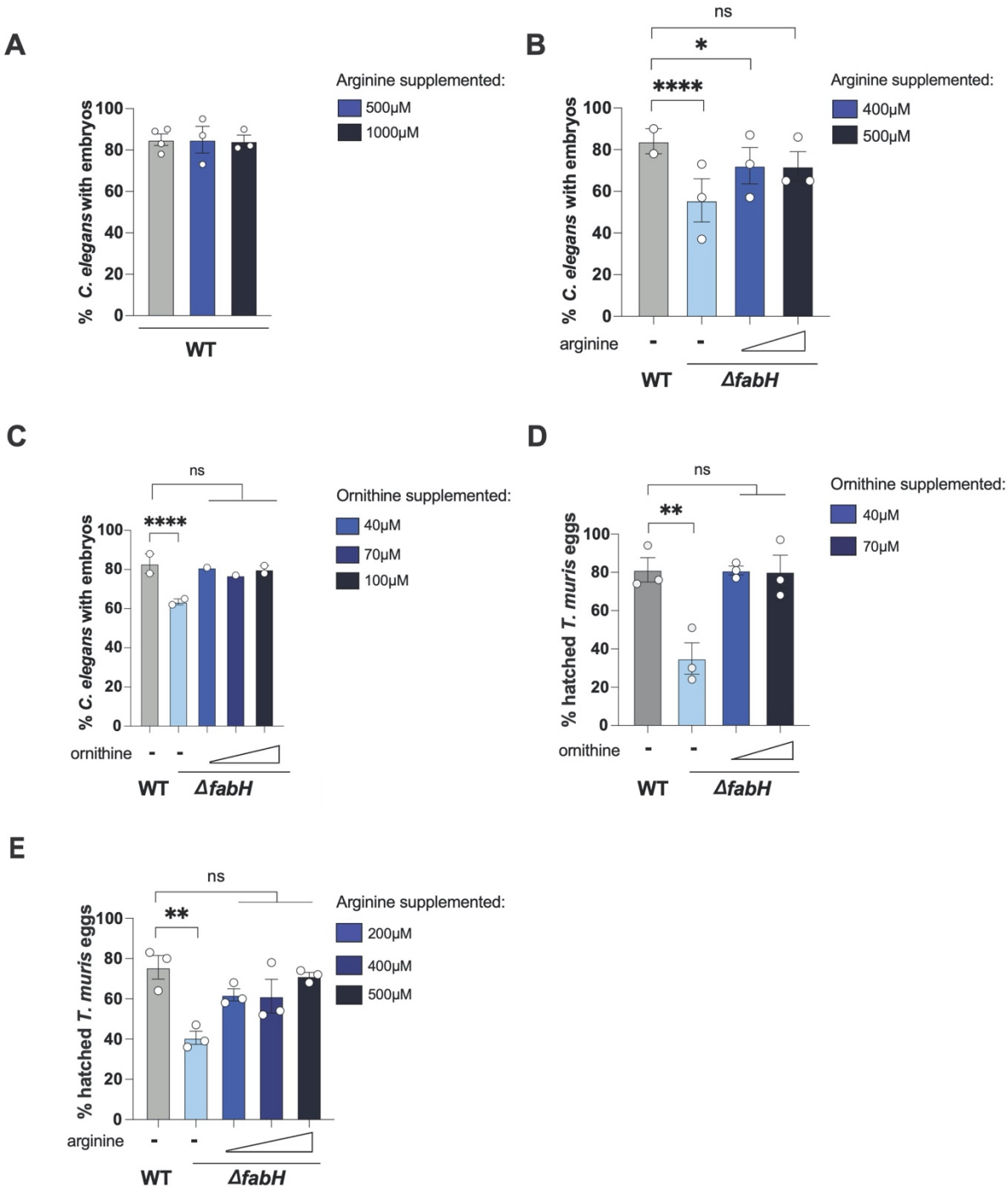

891

892 **Fig. S4 Ornithine or arginine supplementation of Δ*fabH E. coli* rescues defects in**
893 ***C. elegans* and *T. muris*, related to Fig. 2. (A-C)** Percentage of *C. elegans* Day 1
894 adults with embryos; WT = WT *E. coli*. **(A)** Arginine supplementation does not alter

baseline penetrance of *C. elegans* with embryos in *glp-1(e2141).* Total n worms scored (left to right): 173, 118, 108. **(B-C)** Reproduction of Fig. 2, E-F with additional concentrations of (B) arginine and (C) ornithine. Total n worms scored (left to right) for (B) are 208, 237, 200, 300 and (C) 207, 216, 39, 20,149; p values calculated by Fisher's exact test. **(D-E)** Reproduction of Fig. 2, G-H with additional concentrations of (D) ornithine and (E) arginine. Percent *in vitro* hatched *T. muris* eggs elicited by *E. coli* cultures indicated (n=3). One-way analysis of variance (ANOVA) with Dunnett's post-test compared with WT. For all panels, measurements were taken from distinct samples. The average per independent experiment for two to three technical replicates shown. Graphs show means and SEM. * $p < 0.05$, ** $p < 0.01$, **** $p < 0.0001$. ns = not significant.

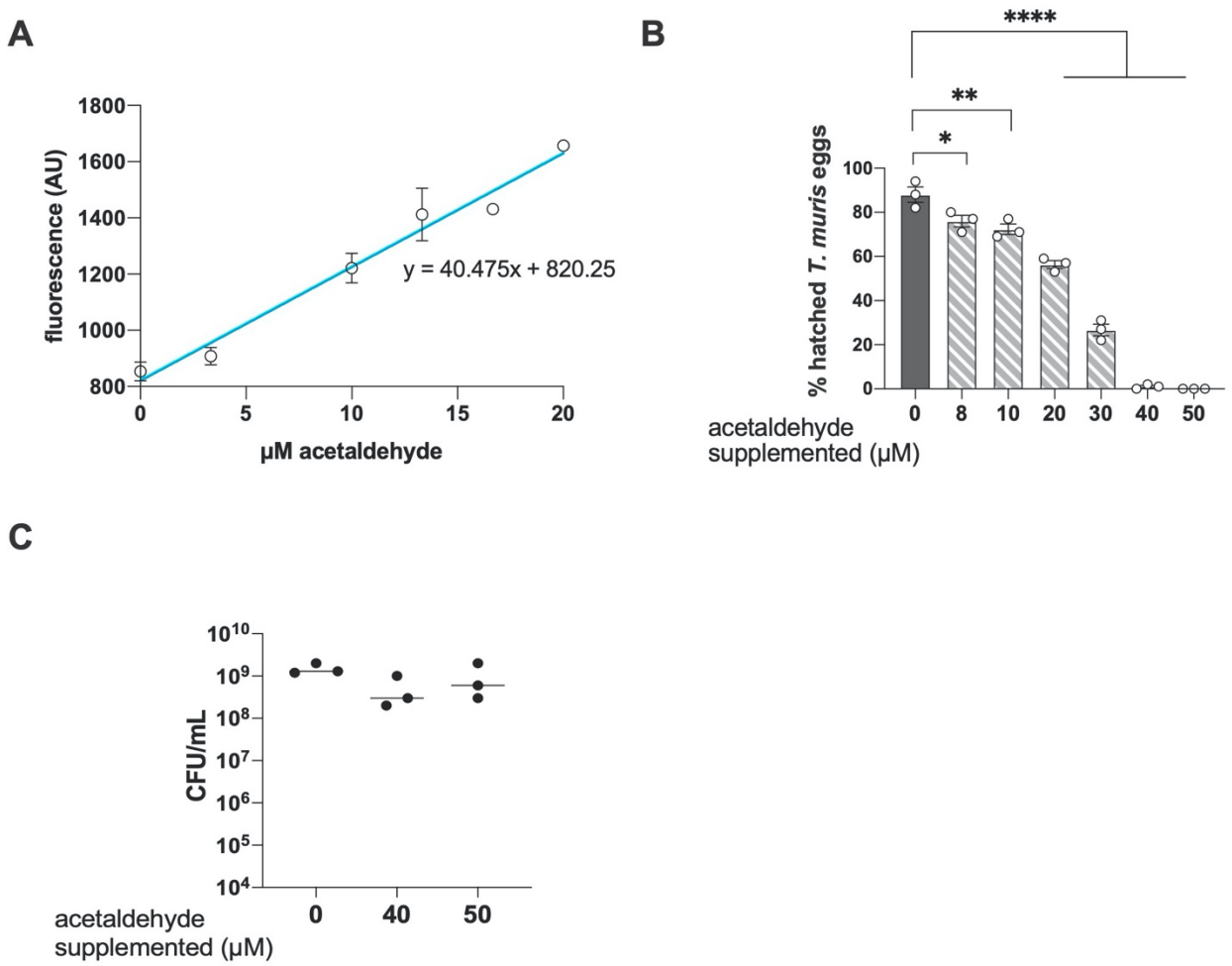

Fig. S5 Acetaldehyde is sufficient to reduce egg hatching, related to Fig. 3.

(A) DarkZone standard curve for acetaldehyde. Fluorescence intensity of samples incubated with known concentrations of acetaldehyde and 20µM DarkZone dye (n = 2). AU, arbitrary units. **(B)** Hatching rates for *T. muris* eggs incubated with WT *E. coli* cultures supplemented with acetaldehyde at concentrations indicated (n = 3). **(C)** Bacterial density of conditions indicated from B measured by dilution plating (n = 3). Measurements were taken from distinct samples. Graph shows means and SEM. B-C, One-way analysis of variance (ANOVA) with Dunnett's post-test compared to 0. * $p < 0.05$, ** $p < 0.01$, **** $p < 0.0001$.

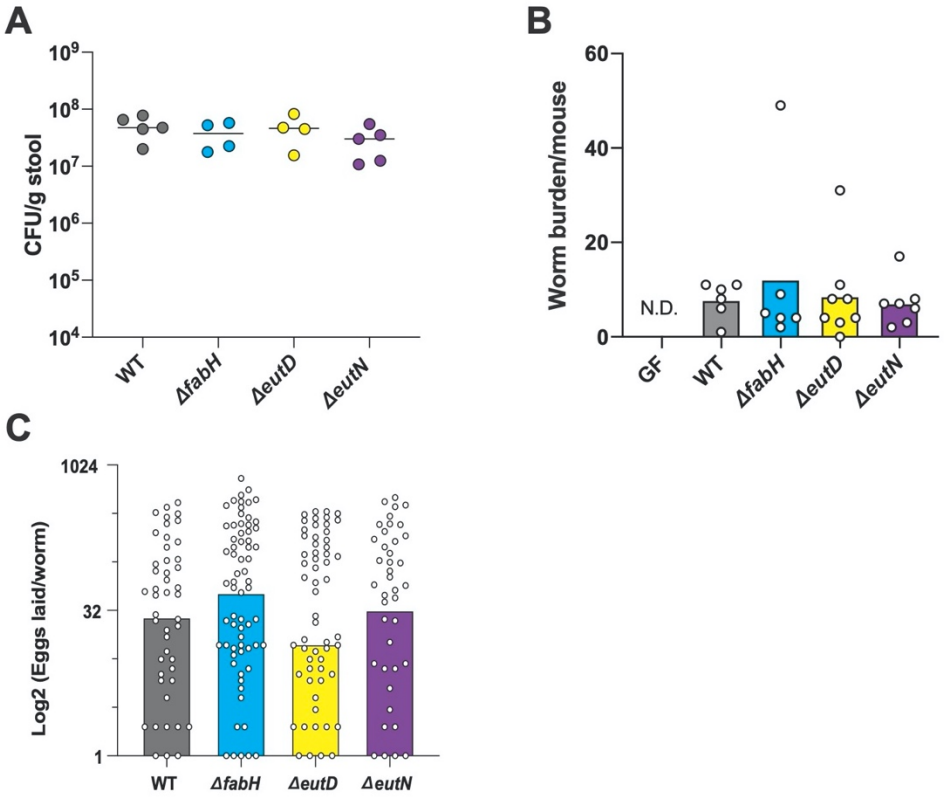

916

917 **Fig. S6 *T. muris* infection of germ-free and monocolonized mice, related to Fig 4.**

918 **(A)** *E. coli* burden 7 dpi in stool of mice gavaged with 1X 10^8 CFU of strains indicated (n

919 = 4-5 mice per group). **(B)** Total worms harvested per mouse for germ-free (GF) and

920 mice monocolonized with *E. coli* strains indicated; N.D. = not detected (n = 6-9 mice per

921 group). **(C)** Quantification of eggs laid per worm. Harvested worms were incubated in

922 individual wells of a 48-well plate with RPMI medium overnight and eggs laid were

923 quantified using light microscopy. Measurements were taken from distinct samples.

924 Graph shows means (A-B) or medians (C).

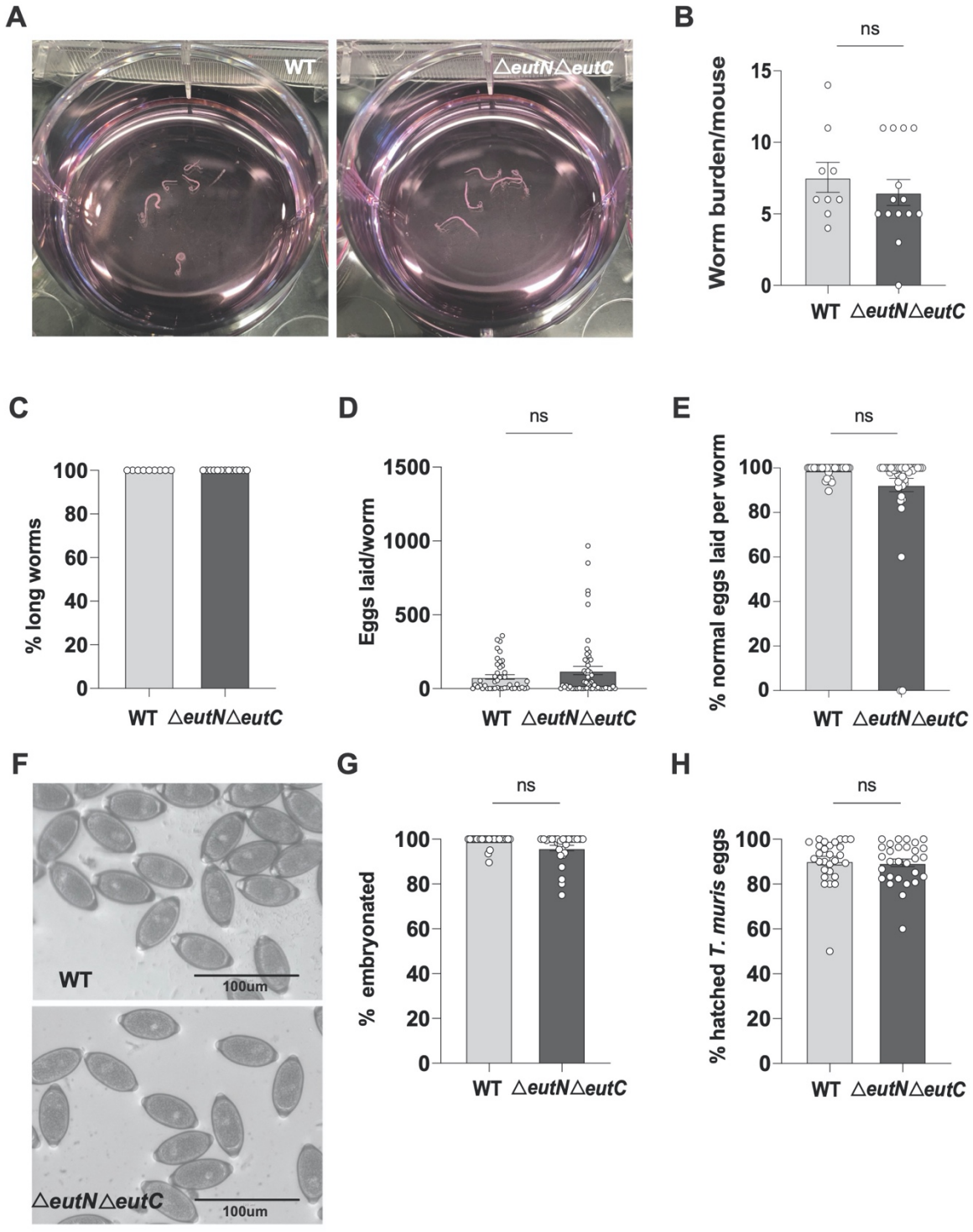

925

926 **Fig. S7 Deleting *eutC* reverses *T. muris* fitness defects induced by Δ*eutN E. coli* in**
927 **mice. (A)** Representative photos of worms harvested from WT and *ΔeutNΔeutC*
928 monocolonized C57BL/6 mice. **(B)** Total worms harvested per mouse for
929 monocolonized groups indicated. Circles represent individual mice (WT, n = 9;

930 *ΔeutNΔeutC*, n = 11). **(C)** Proportion of long worms (> 1cm) harvested per mouse. **(D)**
931 Quantification of eggs laid per worm. Harvested worms were incubated with RPMI
932 media overnight and eggs laid were quantified using light microscopy. Circles represent
933 individual worms (WT, n = 43; *ΔeutNΔeutC*, n = 57). **(E)** Proportion of total eggs laid per
934 worm in (D) with normal morphology**. (F)** Representative images of eggs laid by worms
935 harvested from monocolonized mice groups indicated**. (G)** Percentage of embryonated
936 eggs following 8-week incubation. **(H)** Percentage of eggs in (G) that hatched after
937 incubation with WT *E. coli* for 4 hours at 37°C. (B-E, G-H) Two-tailed, unpaired t-test. ns
938 = not significant. Data shown are pooled from two independent experiments.
939 Measurements were taken from distinct samples. Graph shows means and SEM.

940 **Table S1 Top candidates and bacterial gene function (EcoCyc).** *Fab* and *eut* genes
941 were chosen for further characterization.
942

GENE	PROTEIN FUNCTION	FUNCTIONAL GROUP
fabF	β-ketoacyl-[acyl carrier protein] synthase II	Fatty acid biosynthesis
fabH	β-ketoacyl-[acyl carrier protein] synthase III	Fatty acid biosynthesis
eutD	phosphate acetyltransferase	Ethanolamine utilization
eutN	putative ethanolamine catabolic microcompartment shell protein	Ethanolamine utilization
pta	phosphate acetyltransferase	Ethanolamine utilization
rfaF	ADP-heptose—LPS heptosyltransferase 2	Lipopolysaccharide biosynthesis
rfaH	transcription antiterminator RfaH	Lipopolysaccharide biosynthesis
cmoA	carboxy-*S*-adenosyl-L-methionine synthase	Uridine modification in RNA
yhgN	putative inner membrane protein	Antibiotic resistance
holD	DNA polymerase III subunit ψ	DNA replication

943

944 **Table S2 Strains used in this study.**

STRAIN	SPECIES	GENOTYPE	REFERENCE
BW25113	*E. coli*	*F-, Δ(araD-araB)567, ΔlacZ4787*(::rrnB-3), *λ-, rph-1, Δ(rhaD-rhaB)568, hsdR514*	(*39*)
GC833	*C. elegans*	*glp-1(ar202)* III	(*25*)
GC1250	*C. elegans*	*daf-16(m26) I*; *daf-2(e1370) glp-1(e2141)* III	(*22*)
GC1474	*C. elegans*	*glp-1(e2141)* III; *hjSi20* [*Pmyo-2P::mCherry::unc-54* 3'UTR] IV; *zuIs70* [pJN152: *end-1P::gfp::caax; unc-119*(+)] V	This study
GC1545	*C. elegans*	*daf-5 (e1386) II;glp-1(e2141)* III	This study
GC1547	*E. coli*	BW25113 transformed with pET28	This study
GC1549	*E. coli*	BW25113 Δf*abF*::*kan*	This study
GC1558	*E. coli*	BW25113 Δ*eutN*::kan, pGC735	This study
GC1559	*E. coli*	BW25113 Δf*abH*::kan, pGC738	This study
GC1643	*E. coli*	BW25113 Δ*eutC::kan*	This study
GC1644	*E. coli*	BW25113 Δ*eutC*	This study
GC1645	*E. coli*	BW25113 Δ*eutN::kan*	This study
GC1646	*E. coli*	BW25113 Δ*eutN*	This study
GC1647	*E. coli*	BW25113 Δ*eutC* Δ*eutN::kan*	This study
GC1648	*E. coli*	BW25113 Δ*eutC::kan* Δ*eutN*	This study
JW1077	*E. coli*	BW25113 Δ*fabH::kan*	(*39*)
JW2442	*E. coli*	BW25113 Δ*eutD*::kan	
JW2440	*E. coli*	BW25113 Δ*eutN*::*kan*	
JW2294	*E. coli*	BW25113 Δ*pta*::*kan*	
JW3595	*E. coli*	BW25113 Δ*rfaF*::*kan*	
JW3818	*E. coli*	BW25113 *ΔrfaH*::*kan*	
JW4334	*E. coli*	BW25113 Δ*holD*::*kan*	
JW1859	*E. coli*	BW25113 Δ*cmoA*::*kan*	
JW3397	*E. coli*	BW25113 Δ*yhgN*::*kan*	

945

946

947 **Table S3 Primers used in this study.**

948

Primer	Details
GCo2700 – 5'…. CCGCGCTGGTTCGTTTCtagTGCAGCAATGGCAACAACGTTG	Forward primer- vector fragment to amplify pBR322 for Gibson assembly with PCR product bearing wild-type *fabH* sequence
GCo2701 – 5'…. ACGTTGTTGCCATTGCTGCActaGAAACGAACCAGCGCG	Reverse primer- vector fragment to amplify pBR322 for Gibson assembly with PCR product bearing wild-type *fabH* sequence
GCo2702 – 5'…. AGCTGTCAAACATGAGAATTATAACCGAAAAGTGACTGAGCGTACa	Forward primer- *fabH* coding sequence for Gibson assembly with pBR322
GCo2703 – 5'…. CTCAGTCACTTTTCGGTTATAATTCTCATGTTTGACAGCTTATCATCGATAAG	Reverse primer- *fabH* coding sequence for Gibson assembly with pBR322
GCo2708 – 5'…. agctgtcaaacatgagaattAATACGCCACGGAGGCG	Forward primer- *eutN* coding sequence for Gibson assembly with pBR322
GCo2709 – 5'…. acgttgttgccattgctgcattaTTTGTGGAAAATTACCTGACCGCC	Reverse primer- *eutN* coding sequence for Gibson assembly with pBR322
GCo2710 – 5'…. ACCCGCCTCCGTGGCGTATTaattctcatgtttgacagcttatcatcgataag	Forward primer- vector fragment to amplify pBR322 for Gibson assembly with PCR product bearing wild-type *eutN* sequence
GCo2711 – 5'…. AGGTAATTTTCCACAAAtaatgcagcaatggcaacaacgt	Reverse primer- vector fragment to amplify pBR322 for Gibson assembly with PCR product bearing wild-type *eutN* sequence
GCo2744 – 5'…. GCCGGGAAGCTAGAGTAAGTAGT	pBR322 forward (used to confirm gene sequence)

949

950

951 **Table S4 Plasmid names and descriptions.**

Plasmid name	Description
pGC735	*eutN* cloned into pBR322 by Gibson assembly
pGC737	pET28
pGC738	*fabH* cloned into pBR322 by Gibson assembly
pBR322	pBR322

952

953 **Table S5 Primer sequences to verify kan cassette insertion within target genes.**

GCo296 AGCTTTGAAGTATTACGCCCGGAC	**Forward PCR primer *eutD***
GCo2797 CCTTTCGAGCACGGTCTACG	**Forward sequencing primer *eutD***
GCo2798 AACACCAACCAGCTTGACGC	**Reverse PCR primer *eutD***
GCo2799 AGGCCCCGGGTTTCGATC	**Reverse sequencing primer *eutD***
GCo2800 CTTCCCGATCGGCCTGAAAGG	**Forward PCR primer *eutN***
GCo2801 CTGTAATCACCCTGTGTGACGTCG	**Forward sequencing primer *eutN***
GCo2802 ACTTTGGCTGCCGCAACGGC	**Reverse PCR primer *eutN***
GCo2803 CGCGAAAACGCCCATCTCATG	**Reverse sequencing primer *eutN***
GCo2804 AATTGCCGCTCGCCTGGA	**Forward PCR primer *fabH***

GCo2805 GGTTTTGAGCTGCTGGACGG	**Forward sequencing primer *fabH***
GCo2806 GCCGCAGAAGCTTCAGCAAAC	**Reverse PCR primer *fabH***
GCo2807 GGATAGCTCGCCGCCATATCA	**Reverse sequencing primer *fabH***
GCo2808 GTCCTGCGGTGGTTATCCCAA	**Forward PCR primer *pta***
GCo2809 AAGAACTGGTTATCGCGCAAG	**Forward sequencing primer *pta***
GCo2810 AAGTGGGATGGCGCAATTCAT	**Reverse PCR primer *pta***
GCo2811 GCAGCGCAGTTAAGCAAGATAA	**Reverse sequencing primer *pta***
GCo2812 AATCACCACCGTTCAGGCTGC	**Forward PCR primer *fabF***
GCo2813 GCCACCAGGCGTAAGTGAAC	**Forward sequencing primer *fabF***
GCo2814 CCGTTAATTAAGAACATACCGGCTCC	**Reverse PCR primer *fabF***
GCo2815 AGTGTGGCAGCATGTTCACTACG	**Reverse sequencing primer *fabF***
GCo2832 AACTGAAAGGCCGCTATCAGG	**Forward PCR primer *rfaF***

GCo2833 GGTTACGACAAACCGTTCAAAACC	**Forward sequencing primer *rfaF***
GCo2834 GCCAGGAAGGAATCTGTGCGAA	**Reverse PCR primer** ***rfaF***
GCo2835 CCACCCAGTCAAACTTAATCCCTG	**Reverse sequencing primer** ***rfaF***
GCo2836 GGCGTTCATCTTTGCGATGCTG	**Forward PCR primer** ***rfaH***
GCo2837 CTGACGGTATAACGCAAACCGG	**Forward sequencing primer** ***rfaH***
GCo2838 TCTCACGCCAAAGCCATCATCC	**Reverse PCR primer** ***rfaH***
GCo2839 CCATATTTTGCAACGTATTGCGCAC	**Reverse sequencing primer** ***rfaH***
GCo2840 CTCTTGGCACATCTTTCACCATACA	**Forward PCR primer** ***yhgN***
GCo2841 CGAAGCCATCAGTAATGCGACTT	**Forward sequencing primer *yhgN***
GCo2842 CCGAAACGCTGAAAACCTGGAC	**Reverse PCR primer** ***yhgN***
GCo2843 GGATGATTGCGTTCCAGCTGTT	**Reverse sequencing primer** ***yhgN***
GCo2844 TGTGCGCTGTTGCTGATGGT	**Forward PCR primer** ***cmoA***

GCo2845 TTTGGTATATGCCCTGGGAGTTGG	**Forward sequencing primer** ***cmoA***
GCo2846 GGTAGAAACTCCACCGCATTTGA	**Reverse PCR primer** ***cmoA***
GCo2847 TTAAACAACCCGTGCTGCTGCT	**Reverse sequencing primer** ***cmoA***
GCo2848 TGTGACGCAGCAAGACTTCACT	**Forward PCR primer** ***holD***
GCo2849 ATGCAGACATGGAATGCTCCTCAA	**Forward sequencing primer** ***holD***
GCo2850 ACCACTTGCGTAATCGCAAACG	**Reverse PCR primer** ***holD***
GCo2851 TTGCCGTTTTGCGTTAACTGAAAGT	**Reverse sequencing primer** ***holD***

954